Received 3 April 2025; revised 29 April 2025; accepted 5 May 2025. Date of publication 8 May 2025; date of current version 23 May 2025.

Digital Object Identifier 10.1109/OJCOMS.2025.3568093

Joint Communication and Navigation From LEO Multi-Beam Satellite

ALEJANDRO GONZALEZ-GARRIDO [1] (Student Member, IEEE), JORGE QUEROL [1] (Member, IEEE), HENK WYMEERSCH [2] (Fellow, IEEE), AND SYMEON CHATZINOTAS [1] (Fellow, IEEE)

[1]Interdisciplinary Centre for Security, Reliability and Trust, University of Luxembourg, 1855 Esch-sur-Alzette, Luxembourg
[2]Department of Electrical Engineering, Chalmers University of Technology, 412 96 Gothenburg, Sweden

CORRESPONDING AUTHOR: A. GONZALEZ-GARRIDO (e-mail: alejandro.gonzalez@uni.lu)

ABSTRACT This paper investigates an innovative approach to enable Joint Communication and Positioning (JCAP) in 5G Non-Terrestrial Networks (NTN) using Low Earth Orbit (LEO) multi-beam satellite systems. The integration of communication and navigation services is achieved by aggregating a Direct-Sequence Spread Spectrum (DSSS) as a navigation signal with a 5G Orthogonal Frequency-Division Multiplexing (OFDM) waveform for communication services. Two models are proposed for resource allocation and signal aggregation, referred to as the shared beam model, where communication and navigation signals are aggregated prior to Digital Beamforming (DBF) within the same beam; and the independent beam model, which employs separate beams for communication and navigation, with the navigation beam designed to be significantly wider than the communication beams, resulting in overlap between the two. The performance of these models is assessed using as Key Performance Indicators (KPI) the Cramer-Rao Lower Bound (CRLB) for range estimation used in navigation and the spectral efficiency for the broadband service. The study formulates and addresses a multi-objective optimization problem to derive the Pareto front, highlighting the trade-off between communication and navigation performance. Extensive simulations demonstrate the efficacy of the proposed models in terms of spectral efficiency and accuracy in range estimation, and results have been compared with those obtained from the current 5G positioning system. The models have been evaluated in two distinct scenarios: one without frequency reuse between beams and another incorporating a three-color frequency reuse scheme. The results indicate that the independent beams model outperforms the shared beams model by reducing inter-beam interference in both scenarios. The proposed solution maintains backward compatibility with existing 5G NTN, facilitating uninterrupted positioning and communication services in GNSS-denied environments. Furthermore, the combination of DSSS and OFDM enhances the reliability of the data service by utilizing the DSSS sequence as a digital signature for the waveform. This work establishes a foundation for robust and efficient JCAP implementations, addressing challenges related to multi-beam interference and resource optimization.

INDEX TERMS Joint communication and positioning, 5G NTN, DSSS, digital beamforming, LEO satellite, LEO-PNT, GNSS-free NTN operation.

I. INTRODUCTION

IN THE fifth generation (5G) new radio (NR) non-terrestrial network (NTN) scenario utilizing satellites as next generation base station (gNB), it is essential for the user terminal to incorporate a global navigation satellite system (GNSS) receiver to ensure synchronization with the satellites and to maintain a common time reference [1], [2]. Consequently, the service offered by the satellite network operator relies on a third party, the GNSS, which is beyond its control. therefore, in areas where GNSS is unavailable, network operators are unable to provide their services as users cannot synchronize with the satellites. These GNSS denied areas are regions where connectivity in line of sigh (LOS) with the satellites is available but, with the GNSS service being unavailable, for instance, due to jamming or spoofing attacks. Another scenario in which GNSS is

unavailable involves large-scale Internet of Things (IoT), as incorporating a GNSS receiver into each device could undermine the business model due to the additional costs associated with its inclusion.

A. STATE OF THE ART ON JCAP

An alternative to the use of GNSS for synchronization is to integrate communication services and navigation services within the same satellite infrastructure. This can be achieved by using the pilots in the satellite downlink communication signal. These methodologies are referenced in the literature by various terms, such as integrated communications and localization (ICAL) [3] or joint communication and positioning (JCAP) [4], [5], [6], [7]. The pilots embedded within the data are employed to estimate the user's localization. Although there is no consensus on the acronym, the fundamental concept remains unchanged: to combine communication and navigation services within the same infrastructure.

Some authors utilize communication pilots for positioning in an opportunistic manner, where the systems were not specifically designed for localization purposes [8], [9], [10], [11]. These systems should not be confused with a JCAP system, as the latter was developed specifically for communication purposes. In this work, we propose a JCAP system that is designed to provide both services without adopting an opportunistic approach.

In order to establish a JCAP system, data and navigation signals must share resources during transmission, including time, frequency, or space. In a multi-beam satellite scenario, the designer must meticulously plan the system parameters to minimize interference between beams and services. This planning is critical for ensuring efficient communication, maximizing system capacity, and providing precise positioning services [12]. The following outlines how interference is managed in actual systems and the techniques employed in multi-beam satellites:

- *Frequency reuse with spatial isolation* [13]. Adjacent beams often use different carrier frequencies to minimize interference with typical values of 18-25 dB reduction. This is similar to how terrestrial cellular networks operate, where frequencies are reused in non-adjacent cells [14].
- *Beam Shaping and directional antennas* [15]. The satellite uses a high-gain and narrow beams focusing the signal energy toward specific areas, reducing spillover into adjacent beams. Another alternative is by using adaptive beamforming that adjusts antenna patterns dynamically to optimize coverage and minimize interference with other beams [16] the isolation typical values are about 18-25 dB.
- *Coordinated Beam Scheduling* [12], [17]. The system switches beams on and off in a controlled manner to serve different areas at different times, reducing simultaneous interference. This also includes traffic management by prioritizing and scheduling transmissions based on demand and interference conditions. In this case, the aggregate interference levels can rise to 25-30 dB.

In the previous interference management techniques, each beam carries a single service defined by the transmitted waveform, while interference between services is managed at beam level, independent of the waveform utilized. At this moment, when the network operator wants to offer both services, communications and navigation, the technique for JCAP is based on the inclusion of pilot sequences within the orthogonal frequency-division multiplexing (OFDM) grid for localization purposes [3], [6], [18], [19]. Therefore, the maximum throughput is compromised due to the overhead associated with navigation (pilots).

To reduce the overhead on the OFDM transmission, there is another technique known as superimposed pilots [20], [21], [22], [23]. In this approach, the pilots are combined with the data symbols prior to the OFDM modulation, thereby eliminating the overhead associated with the navigation service. The primary drawback of superimposed pilots is that it requires the receiver to demodulate the signal in order to estimate the channel using these pilots. Furthermore, to successfully demodulate an OFDM signal, coarse synchronization must be performed a priori; typically, this is achieved through the use of training sequence such as the primary synchronization signal (PSS) and secondary synchronization signal (SSS) in 5G NTN [24].

In addition, other works have also considered the integration of direct-sequence spread spectrum (DSSS) and OFDM within the same waveform [25], [26]. The fundamental distinction between these approaches and our proposal lies in the modulation architecture. In the aforementioned works, the data is first modulated using DSSS and subsequently mapped onto the OFDM resource grid. Consequently, the receiver must demodulate the OFDM signal first and then recover the DSSS signal in a cascaded manner. In contrast, our approach adopts a different strategy: the communication data is modulated directly using OFDM, while the navigation component is derived from a DSSS spreading process, thereby enabling concurrent and decoupled processing of both services.

Furthermore, there are some works related in the industry [27], [28], [29]. However, these works provide only navigation services from low earth orbit (LEO) satellites while other works [30], [31] provide navigation services through communication satellites but adopt an opportunistic approach.

Besides, there exists a standardized JCAP system designed by China mobile multimedia broadcasting (CMMB) [32] for terrestrial video broadcasting services. This system use an OFDM waveform for video broadcasting, and additionally, incorporates a navigation signal for localization purposes. The work presented in [33] discusses the aggregation of the

TABLE 1. Waveform comparison for joint communication and positioning systems.

Waveform	Reference	Accuracy	Spectral Efficiency	Robustness	Complexity
OFDM	[36], [37]	Moderate (m-level)	High	Moderate-to-Low	Moderate
DSSS	[37]	High (cm-level)	Moderate-to-Low	Very High	High
DSSS-OFDM Hybrid	This work and [34]	High (sub-m-level)	Moderate-to-High	High	High
TC-OFDM	[38], [33]	Moderate-to-High	Moderate-to-High	Moderate	Moderate
CSS	[39], [40]	High (cm-level)	Low-to-Moderate	Very High (Doppler, Multipath)	Moderate-to-High
FHSS	[41]	Moderate	Low-to-Moderate	High (Interference)	Moderate-to-Low
OTFS	[42]	Moderate	High	High	High
DFT-s-OFDM	[43]	Moderate	moderate	High	High

OFDM signal with the navigation signal, assuming a power level difference of 18 dB between the two signals. Other recent research [34] proposes a similar strategy to deliver navigation and data services by aggregating a DSSS signal onto the OFDM signal; in this case, the author employs a power ratio of 16 dB between the data and navigation signals.

1) WAVEFORMS COMPARISONS

Here we present a qualitative analysis of different waveforms used in the literature for JCAP services. Starting to compare our proposal with the use of the positioning reference signal (PRS) in 5G. Positioning accuracy is governed primarily by the received signal-to-interference plus noise ratio (SINR) and the effective signal bandwidth as seen in the Cramer-Rao lower bound (CRLB) [35]. In 5G PRS, the comb-size parameter (with a minimum value of 2) dictates that up to half of the nominal subcarriers carry the PRS sequence, so the actual PRS bandwidth is at most 50% of the allocated bandwidth. Because our DSSS+OFDM approach uses the full bandwidth continuously, a head-to-head accuracy comparison under equal bandwidth conditions would be inherently unfair. Similar to compare the overhead between our proposal and using 5G PRS, PRS transmissions are managed by the 5G Location Management Function (LMF) and occur in dedicated slots that cannot carry any other data or control information. Consequently, the "overhead" is the fraction of time-slots scheduled for PRS, which varies dynamically with network configuration rather than being a fixed parameter, making it difficult to assign a single overhead value for comparison. Regarding robustness under NTN impairments, both the proposed DSSS+OFDM waveform and the 5G NTN data waveform share the same OFDM structure. The only difference is that our DSSS navigation signal appears as in-band interference to data receivers, effectively capping the maximum SINR depending on the ρ parameter. Below that SINR threshold, however, both schemes exhibit identical performance in the face of Doppler, multipath, and other impairments as the DSSS interference to the OFDM is alike to receiver noise as it is Gaussian.

As a final overview, Table 1 synthesizes the key performance trade-offs of the principal waveforms investigated in the literature for JCAP. It compares each waveform in terms of achievable ranging accuracy, spectral efficiency, resilience to channel impairments and implementation complexity, and it cites representative works where their design and performance are detailed.

In this comparison, DSSS-OFDM hybrids achieve the finest ranging accuracy at the cost of greater implementation complexity, while conventional OFDM and time-coded orthogonal frequency division multiplexing (TC-OFDM) offer high spectral efficiency with only moderate positioning performance. chirp spread spectrum (CSS) and DSSS both provide centimeter-level accuracy and strong robustness against multipath and Doppler effects, though they sacrifices some spectral efficiency. frequency hopping spread spectrum (FHSS) delivers moderate accuracy and robustness with relatively high complexity. And finally orthogonal time frequency space (OTFS) modulation offer a moderate accuracy while the others key performance indicator (KPI) are high.

B. OUR CONTRIBUTIONS

From the previous analysis of the state of the art, we identify some gaps that need to be addressed in order to develop a JCAP system for a multi-beam LEO satellite. Each beam in a satellite typically serves a single service; consequently, a user illuminated by this beam can only receive one service at a time. Most existing JCAP systems based on OFDM suffer from performance degradation due to pilot overhead. In cases involving superimposed pilots, the receiver must first demodulate the received signal. Another limitation of utilizing pilots from OFDM for JCAP is that their application in the NTN scenario may result in reduced accuracy. This reduction appears from the loss of orthogonality between subcarriers, which arises from the significant differential delay and differential Doppler effects characteristic of the satellite environment [44]. Additionally, the standardized CMMB is designed for terrestrial broadcast services, and there is a lack of analysis concerning the power ratio between the broadcast and navigation signals.

To address the previously identified challenges, the main contributions of this paper are outlined as follows:

1) Description and comparison of two different architectures of multi-beam satellite digital beamforming (DBF) to provide a JCAP services. Our first architecture follows a similar approach to the CMMB, aggregating both services within the same transmission. Our second architecture, has a similar approach with the recent work [34].
2) Compare an actual JCAP systems as the 5G PRS with our architectures and discuss the trade-offs of each.
3) Analysis of the proposed waveform based on CMMB TC-OFDM and adapted to the actual 5G NR NTN in a LEO satellite by aggregating a DSSS waveform for localization services.
4) Description on how both signals are time aligned improving the communications service. The navigation signal can be used to detect the start of the OFDM symbol instead of classic algorithms such as [45]. Besides, the communication service can be used for dissemination of the navigation and corrections messages at much higher rate as in assisted GNSS systems.
5) Optimization of the power ratio between the communication and navigation KPIs in order to maximize both services simultaneously by solving the optimization as a Pareto front between both KPIs.

The work presented in this paper uses the communication signal in 5G NR NTN and aggregates a navigation signal based on DSSS similar to the one used in GNSS. Figure 1 shows a representation of the combination of 5G and DSSS aligned with the OFDM symbols. This waveform aggregation presents several benefits to the actual JCAP systems:

- Depending on the user equipment (UE), it can use the baseband processing chain already designed for 5G, other for DSSS, or a combination of both.
- The network operator can offer their communication service in GNSS denial areas by enabling the navigation service.
- Tracking loops in the receiver such as delay locked loop (DLL), frequency locked loop (FLL) and phase-locked loop (PLL) can maintain the lock to the navigation signal more easily compared to burst transmissions, as in the case of OFDM pilots, where not all symbols carry a pilot [46].

C. PAPER ORGANIZATION AND NOTATION USED

This paper is organized into five sections. We begin with this introduction to the problem, followed by Section II where we describe two models of multi-beam satellites, including the channel models, signal models, and SINR models. Next, in Section III we define the KPI for the multi-objective optimization problem and present the details of the Pareto front associated with each model. Section IV presents the simulations conducted to evaluate the performance of the models. Finally, in Section V we summarize the conclusions and outline topics for future research.

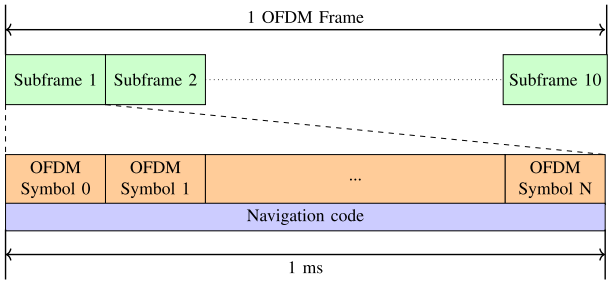

FIGURE 1. OFDM+DSSS combining data transfer and a navigation signal using the 5G Frame structure.

This paper extensively employs mathematical notation, with matrices and vectors represented by boldface uppercase and lowercase letters, respectively. $\mathbb{C}^{m\times n}$ represents the $m \times n$ dimension unitary space. $\otimes$ denotes the Kronecker product. $\circ$ denotes the element-wise product. $\exp\{\cdot\}$ denotes the exponential operator. $[\mathbf{A}|\mathbf{B}]$ represents a matrix composed of two submatrices $\mathbf{A}$ and $\mathbf{B}$ concatenated, where the number of rows is the same. $(\cdot)^T$ represents the transpose of a matrix. Finally, $\text{diag}\{\cdot\}$ denotes a diagonal matrix.

II. SYSTEM MODEL

In this section, we present two architectures, referred to as "Shared beam" ("A" for the mathematical notation) for the model who share the beam for both services, this model is a superposition of both waveforms in baseband. The second model called "Independent" ("B" for the mathematical notation) for the model where the communication and navigation services are at independent beams, but the beams share most of the common illuminated area. In this model, both signals are aggregated at RF, known as over-the-air (OTA).

We begin by presenting the architecture of each model. Then, we provide a detailed description of the channel model, as well as the signals models for both transmission and reception, and the SINR models.

A general assumption is that the beams are intended to be in a fixed angle of departure (AoD), known in the literature as *Earth moving beams* [47].

A. BEAMFORMING NETWORK

We begin by assuming that each model employs a DBF, where the signals for data and navigation can be aggregated in two distinct ways, depending on the model. This DBF control an uniform planar array (UPA) that is oriented always to the subsatellite point (SSP) on the ground. This UPA has $N_t = N_x^{\text{UPA}} \times N_y^{\text{UPA}}$ isotropic radiating elements, where, N_x^{UPA} and N_y^{UPA} are the number of elements on the x and y axis of the UPA. For the sake of simplicity, we assume a square UPA $N_x^{\text{UPA}} = N_y^{\text{UPA}}$. The elements are separated by $\lambda/2$, with λ the wavelength of the transmitted signal.

The UPA response is characterized by the steering vectors $\mathbf{a}(\theta, \phi)$, where the pair $[\theta, \phi]$ represents the AoD of the signal, determined by the azimuth $\theta \in [0, 2\pi)$ and the

elevation angle $\phi \in [0, \pi/2]$ from the UPA plane [3]. The steering vector is defined by $\mathbf{a}(\theta, \phi) = \mathbf{a}^x(\theta, \phi) \otimes \mathbf{a}^y(\theta, \phi)$ as the Kronecker product between the array response in the x axis and the array response in the y axis. Each axis n-th element response is defined as:

$$a_n^x(\theta, \phi) = \frac{1}{\sqrt{N_x^{\text{UPA}}}} \exp\left\{j\pi n u_x\right\} \tag{1}$$

$$a_n^y(\theta, \phi) = \frac{1}{\sqrt{N_y^{\text{UPA}}}} \exp\left\{j\pi n u_y\right\} \tag{2}$$

where $u_x = \sin(\theta)\cos(\phi)$, $u_y = \sin(\theta)\sin(\phi)$ and $n \in \{0, \ldots, \sqrt{N_t} - 1\}$ is the number of elements per row or column in the UPA.

1) SHARED BEAM MODEL

This model also serves as a reference, as the CMMB uses the same approach to combine both signals before their transmission. We have called it *shared beam model*, and it is described in Figure 2. The rationale for this model lies in its compatibility with existing designs, as no modifications are required in the DBF. It can work even as a single beam system.

In this first model, the aggregation of communication and navigation signals is done before the DBF. Consequently, the coverage of the data and navigation service will share the same beam because the aggregated signal uses the same transmission chain (see Figure 2(b)). Additionally, both services experience identical hardware impairments at the transmitter side. This solution facilitates the possibility of having distinct DSSS sequences in the navigation waveform, with one sequence allocated per beam. Moreover, it is cost-effective, as the DBF do not require any dedicated input port for the navigation signal.

The input for the beam k in the DBF can be defined as $s_k[n] = [\sqrt{\rho} \cdot z^{(k)}[n] + \sqrt{1-\rho} \cdot \tilde{z}[n]] \in \mathbb{C}$, where $\rho \in [0, 1]$ is the relative power level between the data $z^{(k)}[n]$ and the navigation $\tilde{z}[n]$ signal. We collect all K beams inputs side-by-side into an array $\mathbf{s}_A[n] = [s_1[n], s_2[n], \ldots, s_K[n]]^T \in \mathbb{C}^{K\times 1}$.

Each of the N_t antennas transmits a linear combination of the K input signals, which is defined in matrix form as

$$\mathbf{x}[n] = \mathbf{W}^{(A)}\mathbf{s}_A[n] \in \mathbb{C}^{N_t \times 1}, \tag{3}$$

where $\mathbf{W}^{(A)} \in \mathbb{C}^{N_t \times K}$ is the steering matrix of the beamforming network (BFN) used to preserve the phase alignment at the reference point of the beams. We choose $\mathbf{W}^{(A)} = \mathbf{A}^*$ as the conjugate of the UPA response for K beams in predefined directions $[\theta_k, \phi_k]$, with $k \in \{1, \ldots, K\}$ defined as $\mathbf{A} = [\mathbf{a}_1, \ldots, \mathbf{a}_K] \in \mathbb{C}^{N_t \times K}$. Here, we simplify the notation of the array response to $\mathbf{a}_k(\theta_k, \phi_k) \triangleq \mathbf{a}_k \in \mathbb{C}^{N_t \times 1}$ by removing the angle dependencies, as each beam k can be distinctly identified solely by the beam number.

2) INDEPENDENT BEAM MODEL

This model follows a similar scheme designed in [34]. This second model is called *independent beams model*. In contrast to the shared beam model, it uses an additional input at the DBF for the navigation service while maintaining the same N_t elements at the UPA. Within this model, the beam designated for the navigation service is considerably wider than the communication beams, with the intent of illuminating as much area as possible. This design choice also indicates that the power received on the ground will be less than that of a spot beam. However, the processing gain of DSSS is very high for sequences like the ones used in GNSS [48]. By leveraging this characteristic the receiver can effectively use the navigation signal even with very low values of SINR.

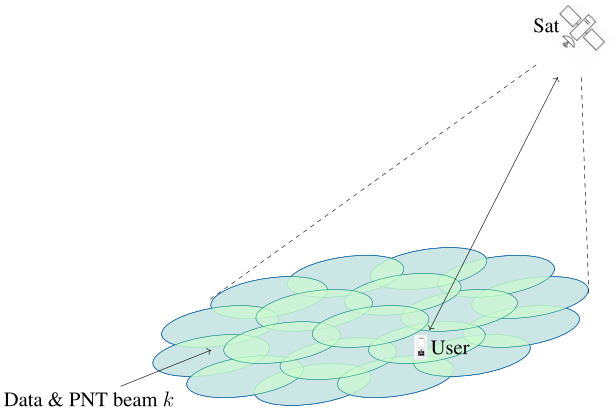

(a) K beams sharing data and navigation service. They all have the same color as all of them transmit the same waveform composed by the DSSS and OFDM.

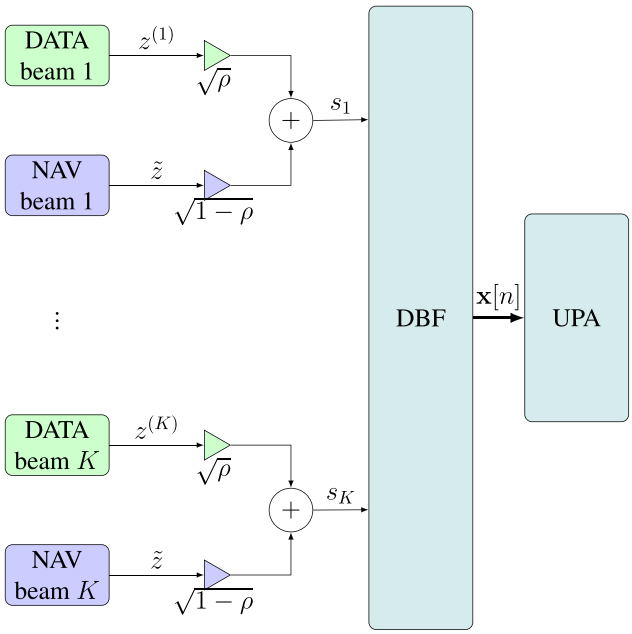

(b) System diagram for K beams. Each beam share a communication (green color) and a navigation (blue color) service as each beam transmission chain is composed by the same elements. The color after the waveforms aggregation represent the combination of green and blue color.

FIGURE 2. Shared beam model.

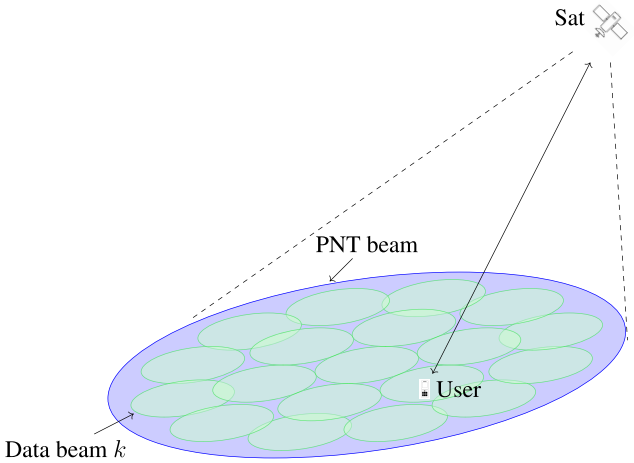

(a) K different beams for data and a single beam for navigation service.

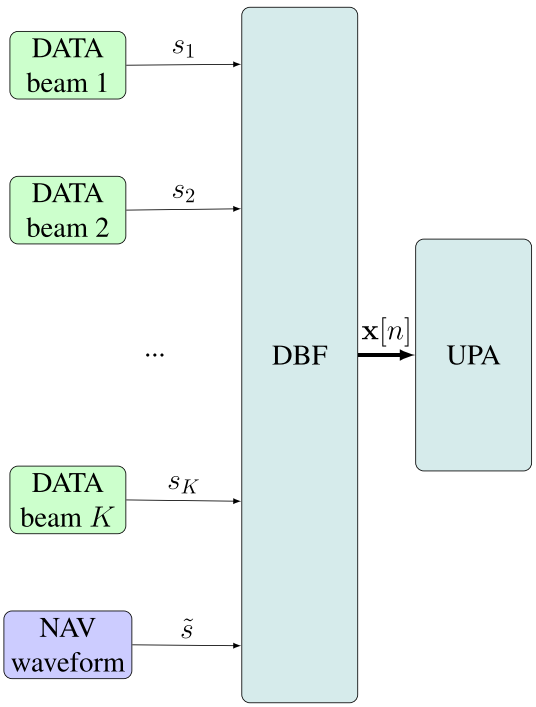

(b) System Diagram. Each data beam is independent and only one beam for navigation services that is independent from the data beams.

FIGURE 3. Independent beam model.

Figure 3 illustrates the independent beam model. In this scenario, the signals are transmitted across distinct beams (refer to Figure 3(a)), and the aggregation is considered done OTA, as both waveforms still share the same resources (time, frequency, and space).

The independent beam model generates $K+1$ beams, K for the communication service and 1 extra for the navigation service. In this work, we assume that the navigation beam and the central beam for communication (the beam aimed at the SSP) has the same AoD $[\theta_1, \phi_1] = [\theta_{\text{NAV}}, \phi_{\text{NAV}}]$. The rationale behind this assumption is our objective to maximize the coverage area for the navigation beam, and pointing towards the SSP will provide the largest field of view (FOV) from the satellite's perspective. However, each of these services have a different beamwidth.

By using different spatial distributions in the UPA, we can customize the shape and width of the beam, even when both beams point in the same direction. Consequently, a narrow beam can be produced by utilizing the full aperture with a uniform amplitude distribution, whereas a wider beam can be generated by modifying the amplitude distribution across the array. There are two methods to accomplish this:

- *Tapering* [49], [50]: Apply an amplitude taper (e.g., a Hamming or Kaiser window) that progressively reduces the amplitude towards the edges of the array. This reduces the effective aperture in a soft manner, broadening the main lobe.
- *Subaperture Use* [51], [52]: Another approach is to effectively use only a central subset of elements to reduce the effective aperture size. A smaller effective aperture leads to a wider beam.

For the design of the steering matrix $\mathbf{W}^{(B)} \in \mathbb{C}^{N_t \times K+1}$ we use the conjugate of the array response, similar to the shared beams model $\mathbf{W}^{(B)} = \mathbf{A}^*$. Then, for this model we choose the *subaperture use* method for the navigation beam, as it generally provides better overall high power amplifier (HPA) efficiency, allowing subarray's amplifiers to run closer to saturation [53], [54]. Therefore, the steering matrix $\mathbf{W}^{(B)}$ can be defined as $\mathbf{W} = [\mathbf{w}_1, \ldots, \mathbf{w}_K, \mathbf{w}_{\text{NAV}}]$, where each $\mathbf{w}_k \in \mathbb{C}^{N_t \times 1}$ are the weights for each beam. The navigation beam is now defined as $\mathbf{w}_{\text{NAV}} = [0, \ldots, w_u, w_{u+1}, \ldots, w_{u+j}, \ldots, 0]^T$, where most of the elements are be 0, except for the subset $\mathcal{U}$ of $j < N_t$ radiating elements used for the wide beam.

Then, as the navigation beam intentionally interferes with the communication beam, different power levels should be applied to each beam to control this intentional interference between services. Here, we assume that each beam transmits sufficient power to achieve a specific SINR at the more distant receiver, which is considered the worst-case scenario that needs to be addressed. Therefore, the DBF is defined as $\mathbf{W}^B = [\rho_1 \mathbf{w}_1, \ldots, \rho_K \mathbf{w}_K, \rho_{\text{NAV}} \mathbf{w}_{\text{NAV}}] \in \mathbb{C}^{N_t \times K+1}$, where ρ_k is the relative power for beam k such that $\sum_{k=1}^{K+1} \rho_k = 1$ (including ρ_{NAV}). The notation is simplified as $\mathbf{W}^{(B)} = \boldsymbol{\rho} \circ \mathbf{W}$, where $\boldsymbol{\rho} = [\boldsymbol{\rho}_{\text{DATA}} | \boldsymbol{\rho}_{\text{NAV}}] \in \mathbb{R}^{N_t \times K+1}$ is the matrix with the relative power for each beam and the elements of each column are equal.

The aggregation of both waveforms is done by adding a new port to the DBF input for the navigation signal $\mathbf{w}_{\text{NAV}}$; therefore, for the input to the DBF we collect them side-by-side into a matrix $\mathbf{s}_B[n] = [s_1[n], s_2[n], \ldots, s_k[n], \tilde{s}[n]]^T \in \mathbb{C}^{(K+1)\times 1}$.

Each of the N_t antennas transmits a linear combination of the $K+1$ input signals, in matrix form is defined as

$$\mathbf{x}[n] = \mathbf{W}^{(B)} \mathbf{s}_B[n] \in \mathbb{C}^{N_t \times 1}. \tag{4}$$

3) MODEL COMPARISON AND CHALLENGES

In this subsection, we present a comparison and the trade-offs for each architecture. We begin with the common benefits, then we describe each architecture particularities and challenges to implement them and finalizing with the trade-offs.

One of the benefits from the aggregation of the DSSS and the OFDM waveforms is the time alignment of both signals, as seen in Figure 1. The receiver can exploit this alignment to detect the start of the OFDM symbol. Classic algorithms such as [45] are widely used to detect the symbol start by using the cyclix prefix (CP) of the OFDM symbol. However, the duration of the CP is usually kept very short to avoid inefficiencies in the transmission, and this short correlation is not reliable in scenarios with low SINR [55]. Therefore, by adding a DSSS aligned with the symbol start, a much larger sequence can be used to find the beginning of the OFDM symbol, improving detection in low-SINR scenarios such as satellite links.

Any multi-beam model can result in frequent handovers since each beam covers a small area and the satellite's motion quickly pushes users from one beam to another [56]. The downside of the shared beam is the potential need to re-acquire or adjust to the new navigation signal, which increases the reacquisition time. Therefore, the independent-beam model provides a wide-area beam for navigation that remains available across multiple spot beams [57]. This can enhance robustness during communication handover. When a user switches communication beams, the broad synchronization beam overlaps and provides a continuous reference, seamlessly transferring their timing lock and facilitating "make-before-break" handovers [57].

As a LEO satellite passes, the path loss and link geometry change constantly. When the satellite is low on the horizon, the range is longer and the signal may pass through more atmosphere. As it comes overhead, the range shortens. These variations can be on the order of dozens of dB over a pass [58]. Additionally, users might experience blockage at low angles. Beamforming networks are often designed for the worst-case (edge of beam, lowest elevation) and ensure "each beam transmits sufficient power to achieve a certain SINR at the most distant receiver" [57]. But with digital control, one can do better than a fixed worst-case design: beams can borrow power or resources from others if needed. This is related to coordinated scheduling; if one beam's link is temporarily bad (e.g., heavy rain or low elevation), the system might allocate it more time slots or concentrate array gain there, while neighboring beams back off [59].

Furthermore, both shared-beam and independent-beam models face common implementation challenges, but they manifest in slightly different ways:

- *Hardware & Complexity:* Shared beams keep hardware count lower (fewer total RF-chains/DACs). Independent beams use an extra beamformer chain increasing the hardware requirements yet offering design flexibility (different beam shapes, separate optimization per service). Mitigation for both lies in advanced DBF, and modular array architectures to manage complexity [60].
- *Power Usage:* Fully digital payloads strain the power budget; shared beams risk extra inefficiency due to multi-signal HPA back-off, whereas independent beams need an additional amplifier but can optimize each beam's power independently. The independent model showed advantages in HPA efficiency by tailoring the nav beam transmission. Mitigation strategies include digital pre-distortion and power control to improve amplifier performance, and intelligent power sharing across beams (whichever model is used) to meet but not far exceed link requirements [61].
- *Synchronization:* Both models must tackle Doppler and timing, a challenge unique to fast LEO orbits. Shared beams deliver per-beam sync, meaning users always get a timing signal from their current beam. Independent beams can broadcast a common nav signal across the coverage, simplifying UE beam handover, but large differential Doppler must still be pre-compensated [57].
- *Interference:* In shared beams, interference is primarily inter-beams as in any multi-beam system. In independent beams, inter-service interference becomes an inter-beam issue. Notably, independent beams has a reduced interference, yielding better accuracy for the navigation service. Traditional interference countermeasures (frequency reuse patterns, polarization isolation) benefit both models [59].
- *Dynamics & Robustness:* The moving satellite scenario stresses both models. Shared beams concentrate all functions in one link, more complex handover [56]. Independent beams distribute functions, which can improve robustness (e.g., continuous nav coverage during comm handover) but adds complexity in time alignment. The independent model's wider beam inherently cover more area, which can be an advantage for providing consistent coverage during beams transitions.

Fully digital beamforming is a double-edged sword for LEO constellations [62]: it provides the tools to address LEO challenges, yet it introduces its own challenges in hardware, power, and design complexity. The shared-beam model leans toward simpler payloads, it piggybacks multiple signals in one beam, but must carefully balance their interaction and might sacrifice some performance to interference and less flexible resource allocation. The independent-beam model grants more freedom, each beam can be optimized and interference between services is reduced, yielding better overall performance at the expense of additional payload resources and coordination of parallel beams.

Finally, Table 2 summarizes the advantages and disadvantages of each model.

B. CHANNEL MODEL

For the channel model we start by assuming that the user's position and velocity remain constant throughout the

TABLE 2. Comparison of shared beam model and independent beam model for joint communication and PNT services.

KPI	Shared beams	Independent beams	Rationale
Cost	✓	×	1 Less DACs and HPAs in the BFN
Flexibility	×	✓	The navigation beam can have a different shape regardless of the data beams
Compatibility	✓	×	It can work with actual payloads without adding new hardware
Performance	×	✓	The aggregated interference created by the navigation beam sidelobes is smaller.
Channel estimation	✓	×	Shared beam transmissions share the effect of the channel for both services.
Reacqusition latency	×	✓	Smaller beams require more re-aquisition of the navigation signal.

measurement interval (1 ms per OFDM subframe in 5G). The parameters driving this model between the UPA and the user are the complex channel gain $g_u = \sqrt{L_u}e^{j\varphi}$ composed by the path loss $\sqrt{L}$ and $\varphi \in \mathcal{U}(0, 2\pi)$. Besides, the channel includes a delay $d \approx \lfloor \tau/T_s + 0.5 \rfloor$, Doppler υ_u and the array factor $\mathbf{a}(\theta_u, \phi_u)$ where (θ_u, ϕ_u) are the direction angles between the UPA and the receiver u from the UPA perspective. To simplify the notation we define $\mathbf{a}^T(\theta_u, \phi_u) \triangleq \mathbf{a}_u^T$. The channel model $\mathbf{h}[n] \in \mathbb{C}^{1\times N_t}$ is described for each antenna in the UPA by

$$\mathbf{h}_u[n] = g_u e^{j2\pi\upsilon_u[nT_s]}\delta[n - d_u]\mathbf{a}_u^T. \tag{5}$$

C. SIGNAL MODELS

1) COMMUNICATION SERVICE

The waveform used for the communication service is the CP-OFDM used in 5G NTN, with a bandwidth of BW Hz, divided in N_{SC} subcarriers. The subcarrier spacing is f_{scs} and the symbol duration is $T_{\text{s}} = \frac{1}{f_{scs}} + T_{\text{cp}}$, where T_{cp} is the duration of the CP. Each OFDM subframe, depending on the numerology used in 5G, will have different number of OFDM symbols. However, the duration of the subframe is fixed to 1 ms. The OFDM carry only user data, modeled as a Complex Gaussian Random Variable with 0 mean and σ^2_{OFDM} variance. We define $\{Z_f^{(k)}\}_{f=0}^{N_{\text{sc}}-1}$ the frequency-domain data symbols (e.g., QAM symbols) assigned to each subcarrier f for the beam k. The discrete-time OFDM signal $\mathbf{z}^{(k)}$ of length N_{OFDM} for beam k is then given by the inverse discrete Fourier transform (IDFT) of the frequency-domain vector $Z_f^{(k)}$ as $\tilde{\mathbf{z}}^k = [z_0^{(k)}, z_1^{(k)}, \ldots, z_{N_{\text{FFT}}-1}^{(k)}]^T \in \mathbb{C}^{N_{\text{FFT}}\times 1}$. Then, it has appended the CP at the beginning of the signal, and considering a rectangular window as pulse shaping, the discrete time data signal is defined as $\mathbf{z}^k = [z_{N_{\text{FFT}}-N_{\text{CP}}}^{(k)}, \ldots, z_{N_{\text{FFT}}-1}^{(k)}, z_0^{(k)}, z_1^{(k)}, \ldots, z_{N_{\text{FFT}}-1}^{(k)}]^T \in \mathbb{C}^{N_{\text{OFDM}}\times 1}$. Finally, the complete input to the BFN for all beams can be written as $\mathbf{Z} = [\mathbf{z}^0, \mathbf{z}^1, \ldots, \mathbf{z}^{K-1}]^T \in \mathbb{C}^{K\times N_{\text{OFDM}}}$.

2) NAVIGATION SERVICE

Now, the waveform used for the navigation service is a DSSS, composed by a low data rate service $\mathbf{b}$, a spread code Υ and a pulse shaping function ξ. The low data rate service bitstream can be modeled as a uniform random variable, defined as $\mathbf{b} = [b_0, b_1, \ldots, b_{N_b-1}]^T \in \mathbb{R}^{N_b-1\times 1}$, where N_b is the number of bits of the navigation message. The spreading code is generated by a Gold sequence, similar to GNSS. It is defined as a block code matrix $\Upsilon \in \mathbb{C}^{N_bN_\kappa\times N_b}$, where each column κ_i corresponds to the spread code for bit i. As the spreading code is fixed for all bits (each satellite or beam has its own code), Υ is constructed by repeating the spreading code along the diagonal. Let $\kappa = [\kappa_0, \kappa_1, \ldots, \kappa_{N_s-1}]^T \in \mathbb{R}^{N_\kappa-1}$ the spreading code for one bit, with $N_\kappa - 1$ as the length of the code, the block diagonal matrix is defined as $\Upsilon = diag\{\kappa\} \in \mathbb{R}^{N_sN_\kappa\times N_s}$

The model for the DSSS waveform is $\tilde{\mathbf{z}} = \Upsilon\mathbf{b}\xi \in \mathbb{C}^{N_sN_\kappa\times 1}$.

3) CONSIDERATIONS FOR THE SIGNAL AGGREGATION

Something to take into account before the aggregation of the OFDM and DSSS signals, is that we must ensure that they are compatible in terms of:

- *Sampling rate* The sampling rate should be aligned at baseband, we define the sampling rate $f_{s,\text{OFDM}}$ for the OFDM signal, and $f_{s,\text{DSSS}}$ for the navigation signal. It is possible to combine both signals by resampling at the maximum common divisor of $(f_{s,\text{OFDM}}, f_{s,\text{DSSS}})$.
- *Signal length (duration)* We design the signal in such a way that the duration of a DSSS sequence and the duration of an 5G OFDM sub-frame are the same; therefore, after the upsampling both signals have the same number of samples.
- *Time alignment (starting point of the signals)* This is designed so that the start of the 5G sub-frame corresponds to the start of a DSSS sequence. Therefore, finding the beginning of one, the receiver knows the start of the other.

In order to have both signal synchronised and aligned, we choose as minimum time unit the 5G Time Unit or T_{c}. Besides, using the concept of T_{c} defined in *TS 38.211 Section 4.1*, we define the duration of a navigation chip as a multiple of this $T_{\text{chip}} = N_{\text{c}} * T_{\text{c}}$, in this way both waveforms are synchronized at sample level.

Furthermore, we want to make both waveforms compatible in terms of the length, therefore we choose the duration of the navigation sequence the same as the 5G subframe $T_{\text{seq}} = T_{\text{subframe}} = N_{\text{chip}}T_{\text{chip}} = N_{\text{chip}}N_{\text{c}}T_u = 1\,ms$, where N_{chip} are the number of chips in the sequence and N_{c} are the number of T_{c}. The value of this two parameters N_{chip} and N_{c} should be calculate in such way that also comply

with the bandwidth of the DSSS waveform as [48]

$$\mathrm{BW}_{\mathrm{DSSS}} \approx \frac{2(1+\alpha)}{N_c T_c}. \tag{6}$$

4) RECEIVED SIGNAL MODEL

The UPA transmission has been defined as $\mathbf{x}[n] = \mathbf{W}^{(\mathrm{MODEL})}\mathbf{s}[n]$, where $\mathbf{W} \in \mathbb{C}^{N_t \times K}$ is the DBF steering matrix, and $\mathbf{s}[n] \in \mathbb{C}^{K\times 1}$ are the K or $K+1$ data streams depending on the model.

We assume that the receiver has a single antenna, therefore, no beamforming from the UE side, as expected by 3rd generation partnership project (3GPP) in its NTN scenario [63]. The received signal for user u can be modeled as

$$y_u^{(\mathrm{M})}[n] = g_u e^{j2\pi \upsilon_u[nT_s]} \mathbf{a}_u^T \mathbf{W}^{(\mathrm{M})} \mathbf{s}^{(\mathrm{M})}[n-d_u] + w_u[n], \tag{7}$$

where $w_u[n] \in \mathcal{N}(0,\sigma^2)$ is the receiver noise. The received signal model in (7) depends on the model used (M in (7)), it can be the shared beams or the independent beams as the steering matrix $\mathbf{W}^{(M)}$ and the modulated signal $\mathbf{s}^{(M)}$ are different.

D. SIGNAL TO INTERFERENCE PLUS NOISE RATIO

From (7) we can split the received signal into three terms, the signal of interest for user u as the beam k with the better performance as $y_{u,k}$; the rest of the beams sidelobes are treated as interference as $y_{u,:}$ and the receiver noise w_u. Therefore, we rewrite the expression from (7) as

$$y_u^{(\mathrm{MODEL})}[n] = y_{u,k}[n] + y_{u,:}[n] + w_u[n] \tag{8}$$

where the signal of interest defined as

$$y_{u,k}[n] = g_u e^{j2\pi \upsilon_u[nT_s]} \left(\mathbf{a}_u^T \mathbf{w}_k^{(\mathrm{MODEL})}\right) s_k^{(\mathrm{MODEL})}[n-d_u], \tag{9}$$

and the interference term are the rest of the beams defined as

$$y_{u,:} = g_k e^{j2\pi \upsilon_u(nT_s)} \sum_{\substack{k=1 \\ k\neq u}}^{K} \left(\mathbf{a}_u^T \mathbf{w}_k\right) s_k[n-d_i]. \tag{10}$$

Assuming $\mathbb{E}\{|s_u|^2\} = P_u$ as the transmitted signal power from beam u, the signal power received is then

$$\mathbb{E}\{|y_{u,k}[n]|^2\} = L_u |\mathbf{a}_u^T \mathbf{w}_k|^2 P_u, \tag{11}$$

the interference from all other beams (assuming that the signals are uncorrelated)

$$\mathbb{E}\{|y_{u,:}|^2\} = L_u \sum_{\substack{k=1 \\ k\neq u}}^{K} |\mathbf{a}_u^T \mathbf{w}_k|^2 P_k, \tag{12}$$

and the noise power $\mathbb{E}\{|w[n]|^2\} = \sigma^2$.

The SINR received is

$$\mathrm{SINR}_u = \frac{L_u |\mathbf{a}_u^T \mathbf{w}_u|^2 P_u}{L_u \sum_{\substack{k=1 \\ k\neq u}}^{K} |\mathbf{a}_u^T \mathbf{w}_k|^2 P_k + \sigma^2}. \tag{13}$$

Now, depending on the signal of interest such as data, or navigation, and the model used, the expressions for the SINR can be further simplified.

1) SINR FOR SHARED BEAMS MODEL

This model is characterized by the input signal to the DBF as $\mathbf{s}^k = [\sqrt{\rho}\cdot \mathbf{z}^k + \sqrt{1-\rho}\cdot \tilde{\mathbf{z}}]$. Assuming that both signals are normalized before applying the relative weight ρ. If our interest is the communication service, $P_u = \rho$ and the navigation signal is an extra interference to the previous SINR definition. Therefore, the SINR for the communication service using this model is

$$\mathrm{SINR}_u^{(\mathrm{data})} = \frac{\rho L_u |\mathbf{a}_u^T \mathbf{w}_u|^2}{L_u |\mathbf{a}_u^T \mathbf{w}_u|^2 (1-\rho) + \rho L_u \sum_{\substack{k=1 \\ k\neq u}}^{K} |\mathbf{a}_u^T \mathbf{w}_k|^2 + \sigma^2}, \tag{14}$$

The SINR for the navigation service follows a similar definition

$$\mathrm{SINR}_u^{(\mathrm{nav})} = \frac{(1-\rho) L_u |\mathbf{a}_u^T \mathbf{w}_u|^2}{\rho L_u \sum_{k=1}^{K} |\mathbf{a}_u^T \mathbf{w}_k|^2 + \sigma^2}, \tag{15}$$

2) SINR FOR INDEPENDENT BEAMS MODEL

For this model, the definition of the SINR for each service, assuming that all signal are normalized at the input to the DBF $P_k = 1$, is just the previous definition done in (13), as the navigation beam is in a different beam than the communication beams.

The definition of the SINR for the communications or the navigation beams is:

$$\mathrm{SINR}_u^{(\mathrm{service})} = \frac{L_u |\mathbf{a}_u^T \mathbf{w}_u^{(\mathrm{service})}|^2}{L_u \sum_{\substack{k=1 \\ k\neq u}}^{K} |\mathbf{a}_u^T \mathbf{w}_k^{(\mathrm{service})}|^2 + \sigma^2}, \tag{16}$$

In this case, the weights for each service are within the respective column $\mathbf{w}_i$ at the steering matrix $\mathbf{W}^{(\mathrm{B})}$.

III. SYSTEM OPTIMIZATION

As described in the previous section, to aggregate both services, we apply different weights to each waveform, resulting in (14), (15), (16) for the SINR. The primary challenge addressed in this work is to determine the optimal values of the signals relative power ρ while maintaining a specific level of quality of service (QoS) for both services and then compare both systems.

In this section, we will formulate the KPI to evaluate, outline the optimization problem formulation, specify the constraints that the solution must satisfy, and present the multi-objective optimization problem by finding the Pareto front.

A. SPECTRAL EFFICIENCY FOR DATA SERVICE

For the communication service, we utilize spectral efficiency as a key metric for optimizing the system. In this context, we consider the navigation signal and the other beams signals

to be an external source of interference. We use the spectral efficiency as defined by Shannon:

$$\eta = \log_2\left(1 + \text{SINR}^{(\text{data})}\right) \tag{17}$$

While spectral efficiency provides a system-level metric that is agnostic to the specific receiver implementation, it is important to note that the SINR can also be used to estimate the bit error rate (BER) for a given modulation and coding scheme. In particular, standard analytical expressions exist that relate SINR to BER under idealized channel models, such as additive white Gaussian noise (AWGN) or Rayleigh fading, for common modulation formats (e.g., BPSK, QPSK, QAM). These mappings are widely used in link-level evaluations and provide a means to approximate BER from SINR. However, actual BER performance is also influenced by receiver design aspects such as synchronization, channel estimation, and decoding algorithms, which are not addressed in this system-level analysis. Therefore, while SINR-to-BER relationships are well known and could be used for approximate BER estimation, we focus on spectral efficiency in this study as it offers a more general and receiver-independent performance measure.

B. RANGE ESTIMATION ACCURACY FOR NAVIGATION SERVICE

For the navigation service, the receiver must first estimate the delay τ from the received signal, and later convert it to range. To evaluate its performance, the utilized metric is the CRLB. Following the development on [64], the CRLB for the DSSS received waveform is defined as follows:

$$\text{CRLB}_{\text{range}} = \frac{3T_{\text{chip}}^2 c}{2\pi^2 T_{\text{seq}}\left(1 - \frac{24}{\pi^2}\alpha^2 + 3\alpha^2\right)\text{SINR}^{(\text{nav})}}, \tag{18}$$

where T_{chip} is the duration of a chip, T_{seq} is the duration of the DSSS, and c is the speed of light.

C. PROBLEM FORMULATION

This work aims to design optimal values for two distinct services utilizing two different metrics: communication and navigation. To address this problem, we define a multi-objective function in which spectral efficiency is maximized while CRLB is minimized. Consequently, the multi-objective function is represented as $f{:}\chi \to \mathbb{R}^2, f(\rho) = [-\eta, \text{CRLB}_{\text{range}}]$, where χ denotes the feasible solution space, $\rho \in \chi$ represents the valid solutions (i.e., Pareto optimal solutions), and $f(\rho)$ is the multi-objective function to be optimized simultaneously. The negative sign in η indicates that we are interested in minimize it.

If one observes the metrics in (17) and (18) the reader can see that the optimization parameters depend solely on the SINR of the service. Therefore, we can simplify the objective function by directly maximizing the SINR of the communication and navigation services simultaneously. We redefine the objective function as $f'{:}\chi' \to \mathbb{R}^2, f'(\rho) = [\text{SINR}_u^{(\text{MODEL,DATA})}, \text{SINR}_u^{(\text{MODEL,NAV})}]$, wherein "MODEL" is employed to distinguish the expressions for the SINR relevant to the shared beam model or the independent beam model. Our optimization problem is defined as follows:

$$\rho = \arg\max_{\rho \in \chi'} f'(\rho), \tag{19}$$

where the constraints associated with this problem are $0 < \rho < 1$ and $\eta > 1$ as a smaller value of η does not makes sense in modern broadband communication systems.

Later for the visualization of the results, we change back to the original KPI, the spectral efficiency and the CRLB.

D. PARETO FRONT DEFINITION

The Pareto front represent the tradeoff between both KPIs, where there is no room for improvement of one KPI while decreasing the quality of the other. From the problem formulation in (19), we use the definitions of the SINR for each model. Then, we describe the Pareto front for each model as the optimal solution. Furthermore, to reduce the notation, we define the following parameters, $\Lambda = L_u|\mathbf{a}_u^T\mathbf{w}_u|^2$, $\Xi = L_u\sum_{\substack{k=1\\k\neq u}}^{K}|\mathbf{a}_u^T\mathbf{w}_k|^2$, and $\Phi = L_u\sum_{k=1}^{K}|\mathbf{a}_u^T\mathbf{w}_k|^2$.

1) SHARED BEAM MODEL

By substituting the expressions (14) and (15) into (19), and using the notation of the previous paragraph, the Pareto curve is defined as,

$$\left\{\left[\frac{\Lambda\rho}{\Lambda(1-\rho)+\rho\Xi+\sigma_u^2}, \quad \frac{\Lambda(1-\rho)}{\rho\Phi+\sigma_u^2}\right], \ \middle|\ \rho \in [0,1]\right\}. \tag{20}$$

The expression in (20) correspond to a Pareto front, where there is no room to improvement to one service while decreasing the quality of the other. This indicates that once the minimum SINR is established for one service (either communications or navigation), the maximum achievable SINR, and consequently the performance, for the other service is upper-bounded. Therefore, a trade-off must be determined by the system designer based on the use case requirements to meet.

2) INDEPENDENT BEAM MODEL

The Pareto front for the independent beam model is defined similarly to (20) in (21), where we substitute the SINR functions from (16) with those of the independent beam model.

$$\left\{\left[\frac{\Lambda_{\text{DATA}}}{\Xi_{\text{DATA}}+\sigma_u^2}, \quad \frac{\Lambda_{\text{NAV}}}{\Xi_{\text{NAV}}+\sigma_u^2}\right], \ \middle|\ \rho \in [0,1]\right\}, \tag{21}$$

where the subindex DATA or NAV correspond to the steering matrix for the data or navigation beam.

To have a common way to compare both models, we use the parameter ρ to weight the power for each service as it is done in the shared beam model. In in the independent beam model we have the steering weights $\mathbf{w}_i$, therefore, we

can extract a parameter ρ from each weight such that $\mathbf{w}_i = \rho_i \tilde{\mathbf{w}}_i \forall i \in \{1, \ldots, K+1\}$ in such way that $\sum_i \rho_i = 1$ and choose the navigation weight as $\mathbf{w}_{\text{NAV}} = (1 - \sum_{i=1}^{K} \rho_i)\tilde{\mathbf{w}}_{\text{NAV}}$. This way we can compare the performance of each model using only one parameter.

3) PARETO FRONTS DESCRIPTION

Previously, we described the joint expressions for the optimal SINR for both services. These expressions define a Pareto front dependent on a single power allocation parameter, ρ, which determines the performance balance between communication (spectral efficiency) and navigation (range estimation accuracy). While ρ is often arbitrarily selected in the literature, not all values are practical. For instance, values of ρ that yield $\eta < 1$ result in very inefficient communication services.

By definition, $0 < \rho < 1$, with:

- Higher values of ρ favor communication by allocating more power to the CP-OFDM signal.
- Lower values of ρ favor navigation by allocating more power to the DSSS signal.

Although ρ can theoretically be tuned continuously, practical system constraints impose bounds on its feasible range:

- *Link budget constraints:* The navigation signal requires a minimum power to maintain lock, limiting how high ρ can be.
- *Service-level agreements:* A minimum required data throughput sets a lower bound on ρ.
- *Payload limitations:* In LEO satellites, limited transmit power restricts extreme values of ρ that might starve one service entirely, violating QoS requirements.

The selection of ρ should start from target QoS thresholds, such as:

- A minimum spectral efficiency for data service.
- A maximum allowable positioning error for navigation service.

The optimal operating point lies on the Pareto front, where any deviation degrades at least one service. In real systems, ρ can be dynamically adapted based on mission requirements or user needs. For example:

- In **GNSS-denied environments**, the network can command a lower ρ to boost navigation.
- During **data-intensive periods**, ρ can be increased to favor communication.

Concrete use cases include:

- *Communications-priority mode:* A high $\rho \to 1.0$ prioritizes data throughput, reducing positioning accuracy. This is acceptable in typical broadband services.
- *Navigation-priority mode:* A low ρ improves positioning, as needed in emergency or search-and-rescue operations, accepting lower data rates.

To implement this trade-off in real-time, the system can adopt adaptive power allocation strategies:

- The satellite's beamforming network applies weights to the composite waveform based on optimized ρ values.
- Telemetry and feedback from users allow the network to update ρ periodically to match current demands.

Additional considerations include:

- *Granularity of adjustment:* LEO dynamics require rapid adaptation, but onboard processing is limited.
- *Lookup table approach:* A pre-computed table of Pareto-optimal ρ values indexed by channel/SINR conditions can reduce computation burden.
- *Navigation continuity:* A minimum DSSS power must always be guaranteed for stable tracking, imposing a lower limit on ρ.

In summary, the parameter ρ acts as a control knob navigating the trade-off between communication and navigation. Its optimal value slides along the Pareto front and can be adjusted in real time to meet mission-specific QoS requirements under practical system constraints.

IV. SIMULATIONS

We begin the simulations with a visualization of the SINR for the optimal beam within a defined coverage area. Then we show also the complementary cumulative density function (CCDF) for the same setup but different values of ρ to evaluate its performance. Finally, we find the pareto fronts for different scenario by taking the best SINR (other values of SINR are suboptimal) and evaluating the KPIs.

The simulations will make use of the 3GPP 5G NTN framework, by using the parameters in their document *TS 38.821 Solutions for NR to support non-terrestrial networks (NTN) (Release 16)*. For the satellite parameters we use the set-2 LEO-600, where we change this model antenna pattern for an UPA. For the UE, we use the handheld model.

We compare two reference scenarios, defined by 3GPP in its document TR 38.821 as *Scenario 24* (SC24) and *Scenario 25* (SC25), the main difference between them is that in *Scenario 24* the satellite use full frequency re-use (FFR) between the beams (all beams use the same carrier frequency) and in *Scenario 25* the satellite use frequency re-use factor 3 (FR3) (the operator bandwidth is divided in three subchannels to avoid that contiguous beams transmit at the same carrier). To distinguish them easily instead of using SC24 or SC25 we will denote them by FFR and FR3. The details of this system are provided in the following Table 3.

From the 3GPP framework in Tables 3, we can obtain:

- Number of radiating elements. $N_{t,\text{DATA}} = 16 \times 16$.
- Angular separation of 6 surround beams. $\theta = 7.66°$, $\phi \in [0, 60, \ldots, 300]°$.

Table 4 shows the different scenarios with the signal bandwidth where we have evaluated both models. The rationale for these values is twofold, the larger bandwidth (30 MHz) correspond to the scenarios defined by 3GPP in its document TS 38.821, and the lower BW values correspond to the proposed work [34] as having 30 MHz, as operator, in the n256 NTN band is quite challenging in terms of

TABLE 3. Scenario details.

Description	Symbol	Value
Satellite altitude	h	600 km
Area of observation	A	$15° \times 15°$
Carrier frequency	f_c	n256 (2.2 GHz)
Satellite EIRP density	δ_P	28 dBW/MHz
3GPP Scenario		C2
Number of beams generated	K	$7(+1)$
UPA Gain	G_{SAT}	24 dBi
Beam spacing in UV plane		0.1334
Number of radiating elements NAV. Independent beam model only	$N_{t,\text{NAV}}$	2×2
Radiating elements distance	$[d_x, d_y]$	$\frac{\lambda}{2}$
Data beams separation	$[\theta_k, \phi_k]$	$\theta = 0.1334$ in uv plane $\phi_k \in \{0, 60, \ldots, 300\}$
Power ratio	ρ	$0, \ldots, 1$
Total Signal bandwidth	BW	5-15-30 MHz
UE Noise Figure	NF	7 dB
UE Rx Gain	G_{Rx}	0 dBi
Duration of the sequence	T_{seq}	1 ms
5G Time unit	T_{c}	0.504 ns
DSSS pulse shaping roll-off	α	0.20
Frequency re-use factor	FRF	Option 1:1 FFR and Option 2:3 FR3

TABLE 4. Scenarios bandwidth.

Scenario	BW data	BW NAV	Number of 5G Time units per chip N_c	Number of chips per sequence N_{chip}	$T_{\text{chip}} = N_c T_c$
FFR	30 MHz	30 MHz	160	12288	81.44 ns
FFR	5 MHz	5 MHz	960	2066	483 ns
FR3	10 MHz	30 MHz	160	12288	81.44 ns
FR3	5 MHz	15 MHz	320	6200	161 ns

licensing. Therefore in the FFR mode, the bandwidth for the data service and navigation is the same, while in the FR3 mode the navigation signal use the total bandwidth and the data is divided between the beams. The main impact in the results is that the noise power levels of the receiver will be different for each scenario and service. This Table also includes the parameters to generate the DSSS signal for different bandwidth, this values are obtained to meet $T_{\text{seq}} \approx N_{\text{chip}} T_{\text{chip}}$ and $T_{\text{chip}} \approx 2/BW$ (the 2 in the formula is because the DSSS sequence is real).

A. FULL FREQUENCY RE-USE SCENARIO

Based on the 3GPP *Scenario 24* in TS 38.821, below are the simulation results for the performance of the joint communication and navigation signal using the parameters in Table 3 for each payload model. In this scenario, there is FFR, therefore all beams transmit a signal using the 30 MHz of bandwidth. This scenario is known as single frequency network (SFN), and it is normally used as a broadcasting system [65].

1) SHARED BEAM MODEL

We start with two reference simulations, Figure 4 shows one when $\rho = 1$, there is no navigation signal. Therefore, this system is the standardized by 3GPP as *Scenario 24*

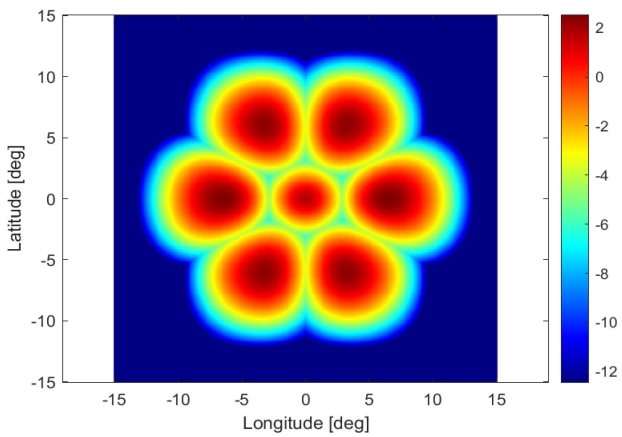

FIGURE 4. FFR. Shared beam model. SINR [dB] reference for the Data beams.

where there is FFR in the beams; and a second simulation in Figure 5 with $\rho = 0$, when only the navigation signal is transmitted through this model. As the system is symmetric from (20), both Figures 4 and 5 are the same.

Then, to evaluate the performance with different values of ρ, Figure 6 shows the CCDF of the SINR in the area of coverage of the beams for different values of ρ. This CCDF represent the percentage of users with a SINR higher than a certain value. We have selected the areas with a

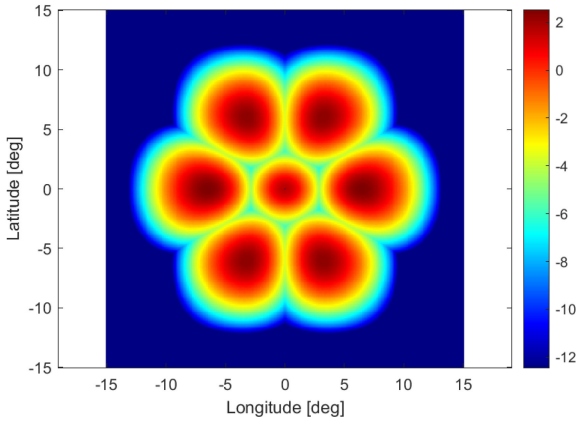

FIGURE 5. FFR. Shared beam model. SINR [dB] reference for the Navigation beams.

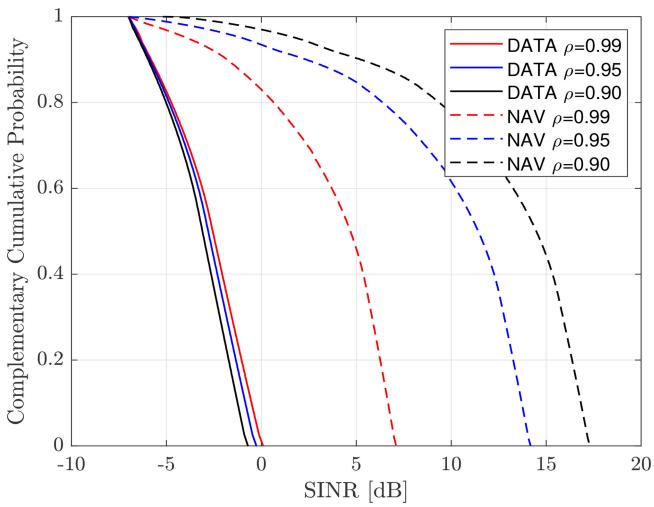

FIGURE 6. FFR. Shared beam model. Complementary Cumulative Density Function of the SINR in the area of interest for different values of ρ.

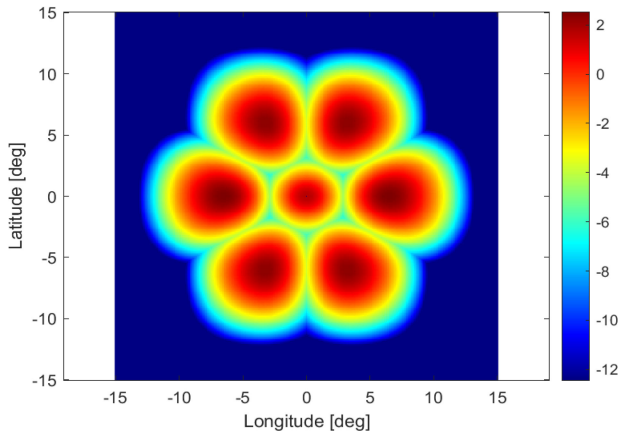

FIGURE 7. FFR. Independent beam model. SINR [dB] reference for the Data beams.

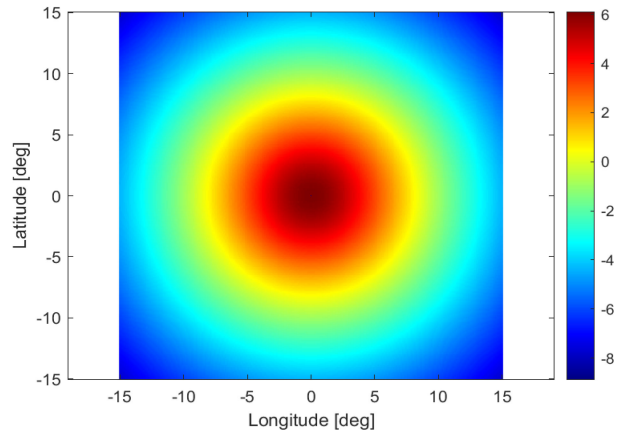

FIGURE 8. FFR. Independent beam model. SINR [dB] reference for the Navigation beams.

SINR ≥ -7 *dB* as is the minimum value to work with before the channel coding gain. Furthermore for the navigation part we have added the correlation gain, that for the sequence length used is 30 dB. It is interesting to see how the CCDF for the data beams remain almost the same for the different values of ρ, while the navigation beams shows an improvement while decreasing ρ.

The improvement in the navigation SINR decreasing the value of ρ can be seen in Figure 6 from the shape of the Pareto front from (20).

2) INDEPENDENT BEAM MODEL

The analysis done for the independent beam model is similar to the analysis done for the shared beam model, it differs as now the navigation beam is much wider and this single wide beam generates interference in all data beams.

Figure 7 shows one when $\rho = 1$, there is no navigation signal. Therefore, this system is the standardized by 3GPP as *Scenario 24* where there is FFR in the beams; and a second simulation in Figure 8 with $\rho = 0$, when only the navigation signal is transmitted through this model. As the system is asymmetric from (21), both Figures 7 and 8 are the now different showing each service a different coverage area.

Then, to evaluate the performance with different values of ρ, Figure 9 shows the CCDF of the SINR in the evaluated area for different values of ρ. It is interesting to see how the CCDF for the data beams remain almost the same for the different values of ρ, while the navigation beams shows an improvement while decreasing ρ. They have a lower SINR than Figure 6 as the surface covered by large power of the navigation beam is larger than in the shared beam model. This can be solved in a future research by designing a isoflux beam for navigation, similar to the ones used by GNSS [66].

The improvement in the navigation SINR decreasing the value of ρ can be seen in Figure 9 from the shape of the Pareto front from (21).

B. FREQUENCY RE-USE FACTOR 3 SCENARIO

In this scenario 25, there is a three color frequency reuse or FR3, therefore the total 30 MHz of the bandwidth is divided in three blocks of 10 MHz according to the *Option 2* from TS 38.821. For the navigation signal, in the independent beam model we still use the 30 MHz.4

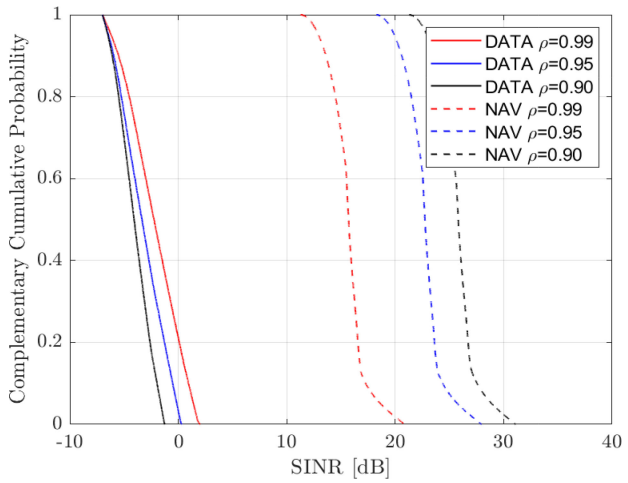

FIGURE 9. FFR. Independent beam model. Complementary Cumulative Density Function of the SINR in the area of interest for different values of ρ.

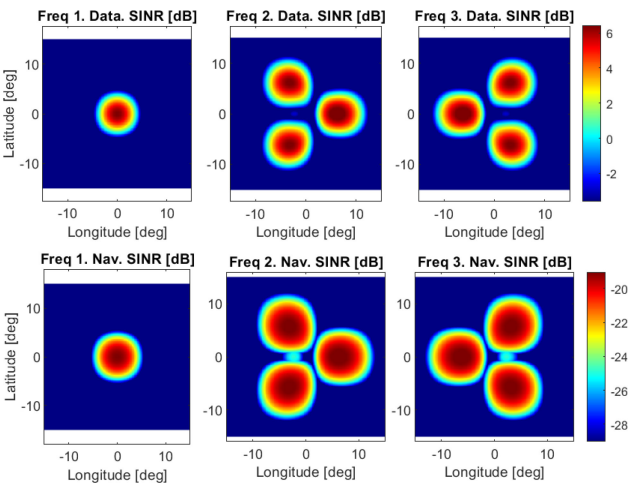

FIGURE 10. FR3. Shared beam model. SINR [dB] reference for the Data and navigation beams.

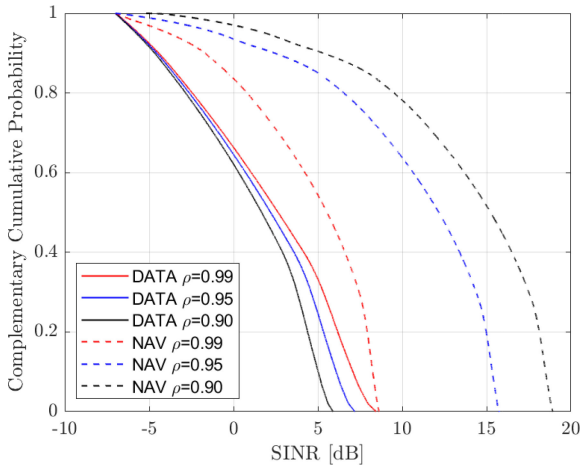

FIGURE 11. FR3.Shared beam model. Complementary Cumulative Density Function of the SINR in the area of interest for different values of ρ.

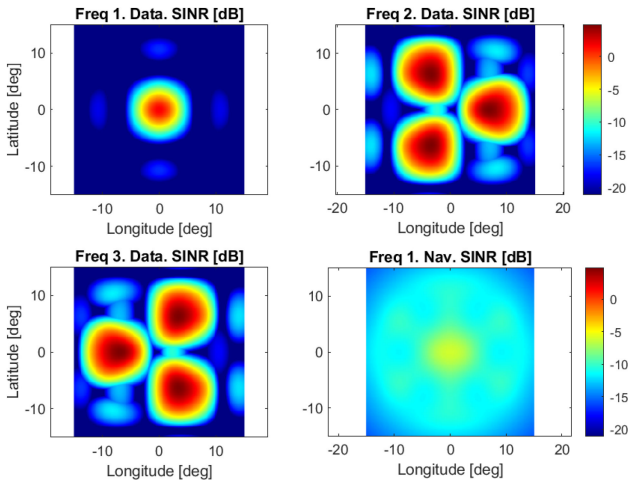

FIGURE 12. FR3. Independent beam model. SINR [dB] reference for the Data and navigation beams.

1) SHARED BEAM MODEL

We start with a reference simulation, Figure 10 shows one when $\rho = 0.98$. Therefore, this system is the standardized by 3GPP as *Scenario 25* where there is a FR3 in the beams.

Then, to evaluate the performance with different values of ρ, Figure 11 shows the CCDF of the SINR in the evaluated area for different values of ρ. It is interesting to see how the CCDF for the data beams remain almost the same for the different values of ρ, while the navigation beams shows a larger improvement while decreasing ρ.

The improvement in the navigation SINR decreasing the value of ρ can be seen in Figure 11.

2) INDEPENDENT BEAM MODEL

We start with a reference simulation, Figure 12 shows one when $\rho = 0.98$. Therefore, this system is the standardized by 3GPP as *Scenario 25* where there is a FR3 in the beams.

Then, to evaluate the performance with different values of ρ, Figure 13 shows the CCDF of the SINR in the evaluated area for different values of ρ. It is interesting to see how the CCDF for the data beams remain almost the same for the different values of ρ, while the navigation beams shows an improvement while decreasing ρ.

The improvement in the navigation SINR decreasing the value of ρ can be seen in Figure 13.

C. RESULTS DISCUSSION, MODEL COMPARISON AND NEXT STEPS TO VALIDATE THE MODELS

The previous simulations to generate Figures 4, 5, 7, 8, 10, and 12 were performed utilizing specific values for ρ. To conduct a comprehensive evaluation of the system, we repeated the simulation with a range of values for ρ.

We use the best SINR obtained at the user terminal for both services for each value of ρ to obtain the spectral efficiency η and the CRLB for the range estimation using the navigation signal. Figure 14 shows the results of the simulation for each model, different values of ρ and the scenario configurations from Table 4. It presents the best

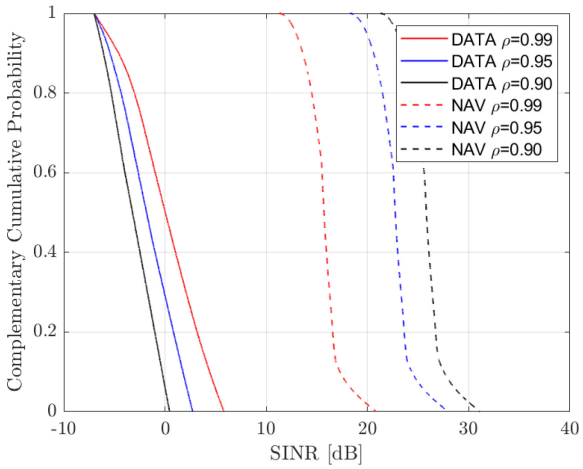

FIGURE 13. FR3. Independent beam model. Complementary Cumulative Density Function of the SINR in the area of interest for different values of ρ.

spectral efficiency achieved for the data signal and the best accuracy on the range estimation using the navigation signals. This result provides insights into the impact of the different parameters on system performance. Furthermore, we have compared the performance with a JCAP system that uses the PRS as a positioning pilots within 5G communication service. The plots of the reference JCAP system are generated by using the definition of spectral efficiency η and the CRLB for the OFDM PRS system, defined as $\eta = (1 - \frac{N_{\text{pilots}}}{N_{\text{total}}}) \log_2(1 + \text{SINR})$ where N_{pilots} are the subcarrier in a symbols dedicated to pilots and N_{total} are the total number of subcarriers. Then for the range estimation we use $\sigma^2_{CRLB} = \frac{6c}{8\pi^2 \text{SINR} \Delta f^2 M N_{\text{pilots}} (N_{\text{pilots}}-2)\ (N_{\text{pilots}}-1)}$, where c is the speed of light, Δ_f^2 is the subcarrier spacing, and M is the number of symbols with the PRS. We assume a subcarrier spacing $\Delta f = 30$ kHz (the one standardized for n256 NTN band), and the number of subcarriers $N = [165, 500, 1000]$ for 5 MHz, 15 MHz and 30MHz.

The results in Figure 14 emphasizes that improving one metric comes at a cost to the other. Solutions below the curve are infeasible, they would require more power than available. Solutions above the curve are sub-optimal. The goal of the multi-objective optimizer is to output the Pareto front, so that system designers can pick an operating point appropriate for the mission (or even schedule different points at different times). For instance, one end of the Pareto front corresponds to maximum navigation accuracy (but poor data rate), and the opposite end to maximum data rate (but poor accuracy). Figure 14 shows this trade-off explicitly: spectral efficiency vs. ranging CRLB is plot for various ρ and highlights how one model or scenario dominates another in different regions. Such Pareto front diagrams are invaluable for designers to visually grasp the compromise and select ρ according to current needs.

Furthermore, the results in Figure 14 only show the values where $\eta > 1$, as values with a spectral efficiency below 1 [bps/Hz] are hardly justifiable by design in modern broadband wireless communications systems. Table 5 shows the minimum value for ρ_{min} to achieve a minimum efficiency of 1 [bps/Hz] and the CRLB achieved at that value of ρ_{min}.

TABLE 5. Minimum usable ρ to get at least $\eta \geq 1$ and the accuracy obtained in the range estimation.

Scenario	Signal BW	Model	ρ_{min}	σ_{range}[cm]
FFR	30/30	Shared beams	0.78	3.49
FFR	30/30	Independent beams	0.94	2.84
FFR	5/5	Shared beams	0.55	1.71
FFR	5/5	Independent beams	0.875	**1.61**
FR3	30/10	Shared beams	0.59	2.36
FR3	30/10	Independent beams	0.88	2.10
FR3	15/5	Shared beams	0.54	1.90
FR3	15/5	Independent beams	0.87	1.77

Table 5 shows a summary of the results: for a FFR scenario with 30 MHz signals (FFR 30/30), to maintain at least 1 bps/Hz data efficiency the power split had to be $\rho \approx 0.78$ (shared-beam model), resulting in a CRLB implying about 3.5 cm range error. Pushing ρ any lower in that scenario caused spectral efficiency to dip below 1 bps/Hz (unacceptable for broadband service).

On the other hand, in a more benign interference scenario (FR3 with 15 MHz data and 5 MHz nav), a balance was found around $\rho \approx 0.54$ for the shared-beam case, yielding 1.9 cm range accuracy at 1 bps/Hz. If ultra-high accuracy were needed, ρ would be tuned even lower – but then the spectral efficiency would drop below the 1 bps/Hz threshold. These numbers demonstrate the practical performance variations: shifting ρ by a few tens of percentage points can swing the spectral efficiency from sub-1 to over 2 bps/Hz. Operators can use such data to decide ρ based on requirements: e.g., if a use-case demands ≤ 1 m accuracy, one must operate on the lower-ρ end of the Pareto front (and tolerate the corresponding throughput reduction).

As the reader can observe in Figure 14 and Table 5 the use of FR3 is outperforming FFR. This is expected as a FFR mode has a large impact in the interference of nearby beams, while FR3 reduces this interference. Now related to the use of a shared or independent beams model, from Table 5 at equal configuration, the independent model outperform the shared beam model. Therefore, the independent model has a higher spectral efficiency. This can be explained as in the shared beam model, each beam transmit two signals, and the side lobes of each beam aggregate reducing the SINR. However, in the independent beam model, for the navigation service, there is only one large beam that generate interference to the data, and only seven beams of data that interfere with the navigation, so the aggregation of the sidelobes signals is much smaller, making this independent beam model a better option for a JCAP system.

It is helpful to quantify how different choices of ρ affect communication and positioning performance. Consider a simplified case with one beam and a fixed total power. If $\rho = 0.8$ (80% power to data), the communication SINR

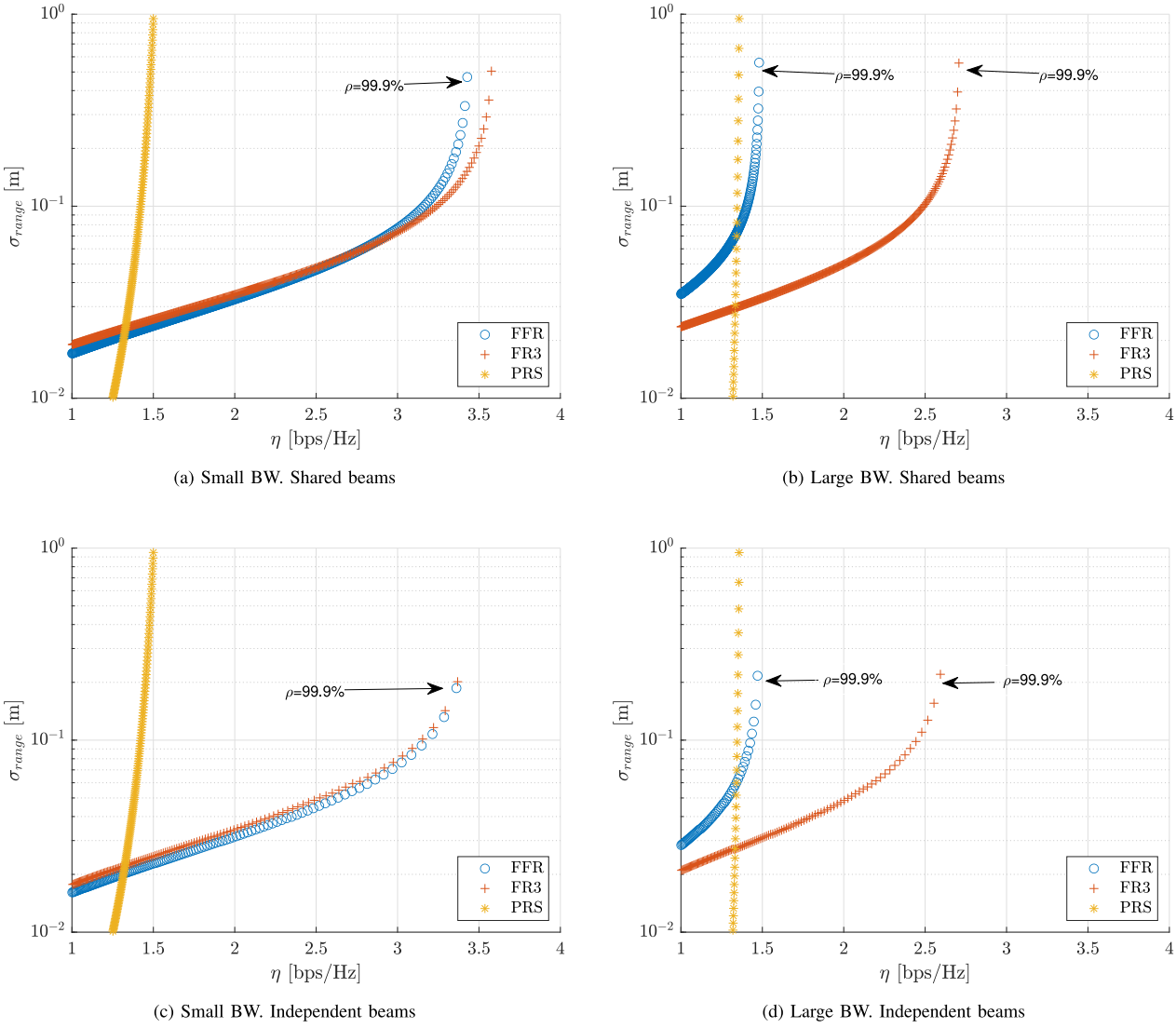

(a) Small BW. Shared beams

(b) Large BW. Shared beams

(c) Small BW. Independent beams

(d) Large BW. Independent beams

FIGURE 14. Spectral efficiency η and CRLB comparison between shared beam model and independent beams in the different scenarios from Table 4. Also for the large bandwidth a comparison from using the 5G PRS as positioning signal.

might be quite high. For instance, plugging into the Shannon formula gives a spectral efficiency on the order of 2 bps/Hz, whereas the navigation SINR is relatively low, yielding a high CRLB (poor accuracy). If we instead choose $\rho = 0.2$ (only 20% to data, 80% to nav), the roles reverse: spectral efficiency drops to about 0.3 bps/Hz while the positioning accuracy improves. This means the range error could be, say, 2–4 times smaller when navigation is prioritized, at the expense of an order-of-magnitude lower data rate.

This system can comply with the accuracy requirements for several of the 5G positioning use cases from [29] and [67] as detailed in Table 6.

1) FUTURE EXPERIMENTAL VALIDATION AND PROTOTYPING STRATEGIES

The current work relies primarily on simulations to demonstrate the feasibility and potential performance advantages of the proposed JCAP scheme. While simulation provides essential initial insights, practical deployment scenarios often present additional complexities not fully captured through simulation alone. Consequently, future work should emphasize experimental validation and prototyping to bridge this gap.

An effective initial step toward validation involves laboratory testing using software defined radio (SDR) to implement and evaluate the proposed DSSS-OFDM aggregation. Such experiments could quantify actual hardware impairments, signal processing delays, synchronization accuracy, and robustness to practical channel conditions, including interference and multipath propagation effects.

Subsequently, transitioning from simulation to a hardware-in-the-loop (HIL) environment would enable rigorous assessment of the JCAP solutions under controlled but realistic operational parameters. This progression from theoretical and simulation-based validations toward practical prototyping experimentation will significantly strengthen the

TABLE 6. Use cases positioning accuracy requirements.

Use case	Expected accuracy	Comply
Emergency Services (eCall)	≤ 1 m	✓
Autonomous Driving	≤ 0.1 m	✓
Industrial Automation	≤ 0.1–0.5 m	✓
Vehicular Navigation	≤ 0.5 m	✓
Augmented Reality	≤ 0.2 m	✓
Drone Navigation	≤ 0.3 m	✓
Precision Agriculture	≤ 0.5 m	✓
Smart City Services	≤ 1 m	✓
Asset Tracking	≤ 1 m	✓
Network verification	≤ 100 m	✓

credibility of the proposed methods and better inform their potential adoption in future satellite communication and navigation systems.

Ultimately, conducting outdoor field trials would provide deeper insights into the real-world performance under realistic propagation and mobility scenarios characteristic of LEO satellite deployments. Collaborations with satellite operators or leveraging existing satellite testbeds would be particularly beneficial for capturing authentic NTN conditions, such as significant Doppler shifts, variable path losses, and intermittent connectivity.

V. CONCLUSION AND FURTHER RESEARCH

In this work, we propose a joint communication and navigation waveform that can be backward compatible with 5G NTN and remove the requirement in the receiver to have a GNSS module. Therefore, the user terminal does not rely on receiving GNSS to access a NTN. Besides, the network operator does not depend on a third party such as GNSS, enabling it to provide services in areas where no GNSS service is available while also offering navigation capabilities.

Through the extensive simulations carried out, we demonstrated the capabilities of the joint waveform to provide a data and a navigation service. The scenario with FFR, still has some value if the receiver integrate some interference cancellation algorithms to improve its SINR, while the scenario with FR3 is more convenient to provide good values for the SINR.

The advantages of this waveform extend beyond enhancing the capabilities of providing JCAP services; the integration of both services within a single receiver yields benefits for each. The data service can leverage the constant navigation signal for the tracking loops, while the navigation service can take advantage of the high data rate of the communication service to convey navigation messages and provide additional assistance to enhance the navigation solution.

Another benefit is the reduction of the overhead in the communications service by reducing the pilot transmissions, as the navigation signal can be used to synchronize the receiver without the need of pilots.

From a standardization perspective, it is important to clarify that the proposed use of DSSS is not intended to replace the 5G waveform (CP-OFDM), but rather to operate on top of it in a transparent manner. In this sense, the DSSS signal can be designed as an overlay that does not interfere with the 3GPP-compliant operation of existing receivers. Therefore, this additional signaling could be defined outside the 3GPP standard and still coexist with standardized communication services, serving specific navigation or authentication functions in a backward-compatible way. The DSSS+OFDM combination aims to enable a GNSS-free operation mode in 5G NTN systems, potentially reducing reliance on third-party positioning systems while maintaining compatibility with current and future 3GPP infrastructures.

As part of future work will be the design of isoflux beams for navigation similar to the ones in GNSS, and evaluate the performance of the tracking loops of a receiver in this framework. Another future work is to explore the feasibility of this waveform combination not only on NTN scenarios, but in terrestrial scenario as a way to integrate terrestrial network (TN) and NTN for the future sixth generation (6G).

Another important direction for future research is the interpretation of DSSS as a digital signature for OFDM signals, as similar to [68]. In this framework, only users possessing the pseudorandom sequence can authenticate the transmitted data. Thus, in the presence of a man-in-the-middle attack, a receiver can verify the integrity of the data, as an attacker without knowledge of the sequence would be unable to generate valid transmissions.

Therefore, the combination of DSSS and OFDM can offer the best of a JCAP plus an increased trustiness on the services.

APPENDIX
ACRONYMS

This paper uses an extensive number of acronyms, and to assist the reader, the following list presents all of them:

3G	third generation
4G	fourth generation
5G	fifth generation
6G	sixth generation
3GPP	3rd generation partnership project
AI	artificial intelligence
AMF	access and mobility function
AoA	angle of arrival
AoD	angle of departure
AR	augmented reality
ASIC	application-specific integrated circuit
AWGN	additive white Gaussian noise
BER	bit error rate
BFN	beamforming network
BO	back-off
BW	bandwidth
C/A	civilian acquisition
CCDF	complementary cumulative density function

CMMB	China mobile multimedia broadcasting
CP	cyclix prefix
CRLB	Cramer-Rao lower bound
CSS	chirp spread spectrum
CU	centralized unit
DAC	digital to analog converter
DBF	digital beamforming
DFT	discrete Fourier transform
DL-AoD	downlink angle of departure
DLL	delay locked loop
DL-OTDoA	downlink observed time difference of arrival
DSSS	direct-sequence spread spectrum
DU	distributed unit
DVB	digital video broadcasting
E-CID	enhanced cell id
ECDF	empirical cumulative density function
E-SMLC	evolved serving mobile location center
EIRP	equivalent isotropic radiated power
eNB	evolved nodeb
EVM	error vector magnitude
FHSS	frequency hopping spread spectrum
FLL	frequency locked loop
FFT	fast Fourier transform
FFR	full frequency re-use
FOV	field of view
FSPL	free space path loss
FR	frequency region
FR3	frequency re-use factor 3
GDOP	geometrical dilution of precision
GPS	global positioning system
gNB	next generation base station
GNSS	global navigation satellite system
GS	ground station
HAPS	high-altitude platform systems
HIL	hardware-in-the-loop
HPA	high power amplifier
IBO	input back-off
ICAL	integrated communications and localization
IDFT	inverse discrete Fourier transform
IFFT	inverse fast Fourier transform
IoT	Internet of Things
IIoT	Industrial Internet of Things
ICI	inter-carrier interference
IMU	inertial measurement unit
ISI	inter-symbol interference
JCAP	joint communication and positioning
KPI	key performance indicator
LCS	location-based services
LEO	low earth orbit
LMC	location management component
LMF	location management function
LNA	low noise amplifier
LOS	line of sigh
LPP	localization positioning protocol
LPPa	localization positioning protocol annex
LTE	long term evolution
MCRB	modified Cramer Rao bound
ML	machine learning
Multi-RTT	multi-cell round trip time
NF	network function
NSGA-II	non-dominated sorting genetic algorithm II
NGSO	non geostationary satellite orbit
NLOS	non-line of sight
NR	new radio
NTN	non-terrestrial network
OFDM	orthogonal frequency-division multiplexing
OTA	over-the-air
OTDoA	observed time differential of arrival
OTFS	orthogonal time frequency space
PAPR	peak-to-average power ratio
PLL	phase-locked loop
PNT	positioning, navigation, and timing
POD	precise orbit determination
PPP	precise point positioning
PRN	pseudo-random noise
PRS	positioning reference signal
PSD	power spectral density
PSS	primary synchronization signal
QoS	quality of service
RAN	radio access network
RAT	radio-access-technology
RB	resource block
RE	resource element
RG	resource grid
RedCap	reduced capacity
RMSE	root mean square error
RTK	real time kinematics
RRC	radio resource control
SBAS	satellite based augmentation system
SDR	software defined radio
SIB	system information block
SIC	sequential interference cancellation
SIR	signal-to-interference ratio
SINR	signal-to-interference plus noise ratio
SFN	single frequency network
SLA	service level agreement
SNR	signal-to-noise ratio
SoO	signal of opportunity
SoP	signal of opportunity
SRS	sounding reference signal
SRRC	square root raised cosine
SSP	subsatellite point
SSS	secondary synchronization signal
TA	timing advance
TC-OFDM	time-coded orthogonal frequency division multiplexing
TDL	tapped delay line
TN	terrestrial network
ToA	time of arrival
ToF	time of flight
TS	technical specification
TR	technical report

UAV	unmanned aerial vehicle
UE	user equipment
UL-AoA	uplink angle of arrival
UL-TDoA	uplink time difference of arrival
UPA	uniform planar array
VR	virtual reality
WLAN	wireless local area network
ZOH	zero-order hold

ACKNOWLEDGMENT

The authors gratefully acknowledge Riccardo di Gaudenzi for insightful discussions and valuable suggestions regarding the technical aspects of this research.

The simulations presented in this paper were carried out using the HPC facilities of the University of Luxembourg [69] (see hpc.uni.lu).

REFERENCES

[1] "Solutions for NR to support non-terrestrial networks (NTN), Version 16.0.0," 3GPP, Sophia Antipolis, France, Rep. TR 38.821, Jan. 2020.

[2] E. Cianca, S. J. Nawaz, C. Amatetti, T. Rossi, and M. De Sanctis, "LEO-based network-centric localization in 6G: Challenges and future perspectives," *Comput. Netw.*, vol. 253, Nov. 2024, Art. no. 110689. [Online]. Available: https://www.sciencedirect.com/science/article/pii/S1389128624005218

[3] L. You et al., "Integrated communications and localization for massive MIMO LEO satellite systems," *IEEE Trans. Wireless Commun.*, vol. 23, no. 9, pp. 11061–11075, Sep. 2024. [Online]. Available: https://ieeexplore.ieee.org/document/10478820/authors#authors

[4] K. Ntontin et al., "A vision, survey, and roadmap toward space communications in the 6G and beyond era," *Proc. IEEE*, early access, Jan. 2, 2025, doi: 10.1109/JPROC.2024.3512934.

[5] A. Shahmansoori, R. Montalban, J. A. Lopez-Salcedo, and G. Seco-Granados, "Design of OFDM sequences for joint communications and positioning based on the asymptotic expected CRB," in *Proc. Int. Conf. Localization GNSS (ICL-GNSS)*, 2014, pp. 1–6. [Online]. Available: https://ieeexplore.ieee.org/document/6934168/

[6] R. C. Adam and P. A. Hoeher, "Simultaneous model and parameter estimation for joint communication and positioning," *IEEE Access*, vol. 9, pp. 2934–2949, 2021.

[7] W. Wang, T. Jost, C. Gentner, S. Zhang, and A. Dammann, "A semiblind tracking algorithm for joint communication and ranging with OFDM signals," *IEEE Trans. Veh. Technol.*, vol. 65, no. 7, pp. 5237–5250, Jul. 2016. [Online]. Available: http://ieeexplore.ieee.org/document/7194841/

[8] W. Stock, R. T. Schwarz, C. A. Hofmann, and A. Knopp, "Survey on opportunistic PNT with signals from LEO communication satellites," *IEEE Commun. Surveys Tuts.*, vol. 27, no. 1, pp. 77–107, 1st Quart., 2025. [Online]. Available: https://ieeexplore.ieee.org/document/10542356

[9] A. Abdallah, J. Khalife, and Z. M. Kassas, "Exploiting on-demand 5G downlink signals for opportunistic navigation," *IEEE Signal Process. Lett.*, vol. 30, pp. 389–393, Jan. 2023. [Online]. Available: https://ieeexplore.ieee.org/document/10009899

[10] K. Shamaei and Z. M. Kassas, "Receiver design and time of arrival estimation for opportunistic localization with 5G signals," *IEEE Trans. Wireless Commun.*, vol. 20, no. 7, pp. 4716–4731, Jul. 2021. [Online]. Available: https://ieeexplore.ieee.org/document/9369049/

[11] K. Shamaei, J. Khalife, and Z. M. Kassas, "Exploiting LTE signals for navigation: Theory to implementation," *IEEE Trans. Wireless Commun.*, vol. 17, no. 4, pp. 2173–2189, Apr. 2018. [Online]. Available: https://ieeexplore.ieee.org/document/8255823/

[12] H. Xv, Y. Sun, Y. Zhao, M. Peng, and S. Zhang, "Joint beam scheduling and beamforming design for cooperative positioning in multi-beam LEO satellite networks," *IEEE Trans. Veh. Technol.*, vol. 73, no. 4, pp. 5276–5287, Apr. 2024. [Online]. Available: https://ieeexplore.ieee.org/abstract/document/10323191

[13] N. Heydarishahreza, T. Han, and N. Ansari, "Spectrum sharing and interference management for 6G LEO satellite-terrestrial network integration," *IEEE Commun. Surveys Tuts.*, early access, Nov. 27, 2024, doi: 10.1109/COMST.2024.3507019.

[14] W. Nam, D. Bai, J. Lee, and I. Kang, "Advanced interference management for 5G cellular networks," *IEEE Commun. Mag.*, vol. 52, no. 5, pp. 52–60, May 2014. [Online]. Available: https://ieeexplore.ieee.org/abstract/document/6815893

[15] P. He et al., "Nonterrestrial network technologies: Applications and future prospects," *IEEE Internet Things J.*, vol. 12, no. 6, pp. 6275–6299, Mar. 2025. [Online]. Available: https://ieeexplore.ieee.org/abstract/document/10816483

[16] P. Bhide, D. Shetty, and S. Mikkili, "Review on 6G communication and its architecture, technologies included, challenges, security challenges and requirements, applications, with respect to AI domain," *IET Quantum Commun.*, vol. 6, no. 1, Jan. 2025, Art. no. qtc2.12114. [Online]. Available: https://ietresearch.onlinelibrary.wiley.com/doi/10.1049/qtc2.12114

[17] S. F. Drampalou, D. Uzunidis, A. Vetsos, N. I. Miridakis, and P. Karkazis, "A user-centric perspective of 6G networks: A survey," *IEEE Access*, vol. 12, pp. 190255–190294, 2024. [Online]. Available: https://ieeexplore.ieee.org/abstract/document/10795171

[18] A. M. Graff, W. N. Blount, P. A. Iannucci, J. G. Andrews, and T. E. Humphreys, "Analysis of OFDM signals for ranging and communications," in *Proc. 34th Int. Tech. Meeting Satellite Div. Inst. Navig. (ION GNSS+)*, 2021, pp. 2910–2924. [Online]. Available: https://www.ion.org/publications/abstract.cfm?articleID=17991

[19] R. Chen, X. Lu, and K. Yang, "Joint resource allocation based on F-OFDM for integrated communication and positioning system," in *Proc. 16th EAI Int. Conf. Commun. Netw.*, 2022, pp. 91–101.

[20] T. Cui and C. Tellambura, "OFDM channel estimation and data detection with superimposed pilots," *Eur. Trans. Telecommun.*, vol. 22, no. 3, pp. 125–136, 2011. [Online]. Available: https://onlinelibrary.wiley.com/doi/abs/10.1002/ett.1461

[21] A. R. Varma, C. R. N. Athaudage, L. L. H. Andrew, and J. H. Manton, "Optimal superimposed pilot selection for OFDM channel estimation," in *Proc. IEEE 7th Workshop Signal Process. Adv. Wireless Commun.*, 2006, pp. 1–5. [Online]. Available: https://ieeexplore.ieee.org/abstract/document/4153906

[22] K. Upadhya, S. A. Vorobyov, and M. Vehkapera, "Superimposed pilots are superior for mitigating pilot contamination in massive MIMO," *IEEE Trans. Signal Process.*, vol. 65, no. 11, pp. 2917–2932, Jun. 2017. [Online]. Available: https://ieeexplore.ieee.org/abstract/document/7865983

[23] D. Bao, G. Qin, and Y.-Y. Dong, "A superimposed pilot-based integrated radar and communication system," *IEEE Access*, vol. 8, pp. 11520–11533, 2020. [Online]. Available: https://ieeexplore.ieee.org/document/8954710/

[24] A. Jayaprakash, B. G. Evans, P. Xiao, A. B. Awoseyila, and Y. Zhang, "New radio numerology and waveform evaluation for satellite integration into 5G terrestrial network," in *Proc. IEEE Int. Conf. Commun. (ICC)*, 2020, pp. 1–7. [Online]. Available: https://ieeexplore.ieee.org/abstract/document/9149274

[25] A. A. Hassan, J. E. Hershey, and G. J. Saulnier, "OFDM spread spectrum communications," in *Perspectives in Spread Spectrum*. Boston, MA, USA: Springer, 1998, pp. 35–58. [Online]. Available: https://link.springer.com/chapter/10.1007/978-1-4615-5531-5_2

[26] P. Tu, X. Huang, and E. Dutkiewicz, "A novel approach of spreading spectrum in OFDM systems," in *Proc. Int. Symp. Commun. Inf. Technol.*, 2006, pp. 487–491. [Online]. Available: https://ieeexplore.ieee.org/document/4141433

[27] F. S. Prol et al., "Position, navigation, and timing (PNT) through low earth orbit (LEO) satellites: A survey on current status, challenges, and opportunities," *IEEE Access*, vol. 10, pp. 83971–84002, 2022. [Online]. Available: https://ieeexplore.ieee.org/document/9840374/

[28] B. Eissfeller, T. Pany, D. Dötterböck, and R. Förstner, "A comparative study of LEO-PNT systems and concepts," in *Proc. ION Pac. PNT Meeting*, 2024, pp. 758–782. [Online]. Available: https://www.ion.org/publications/abstract.cfm?articleID=19646

[29] J. A. D. Peral-Rosado, F. Soualle, A. Hofmann, T. Heyn, J. Querol, and I. Lapin, "Positioning-enabled 5G and 6G satellite networks: Use cases and key technologies," in *Proc. 11th Workshop Satellite Navig. Technol. (NAVITEC)*, 2024, pp. 1–5. [Online]. Available: https://ieeexplore.ieee.org/document/10843544

[30] Z. M. Kassas et al., "Navigation with multi-constellation LEO satellite signals of opportunity: Starlink, OneWeb, Orbcomm, and Iridium," in *Proc. IEEE/ION Posit., Locat. Navig. Symp. (PLANS)*, 2023, pp. 338–343. [Online]. Available: https://ieeexplore.ieee.org/document/10140066/

[31] Z. M. Kassas, "Navigation from low earth orbit part 2: Models, implementation, and performance," in *Position, Navigation, and Timing Technologies in the 21st Century: Integrated Satellite Navigation, Sensor Systems, and Civil Applications*, vol. 2, Hoboken, NJ, USA: Wiley, 2021.

[32] H. ZhaoPeng, H. Yu, C. Hong, Y. ChaoZhong, and Y. JiangBin, "OFDM technology anti-multipath performance analysis in China mobile multimedia broadcasting (CMMB) system," in *Proc. IEEE Int. Freq. Control Symp. (FCS)*, 2014, pp. 1–3. [Online]. Available: https://ieeexplore.ieee.org/abstract/document/6859892

[33] J. Mo, Z. Deng, B. Jia, H. Jiang, and X. Bian, "A novel FLL-assisted PLL with fuzzy control for TC-OFDM carrier signal tracking," *IEEE Access*, vol. 6, pp. 52447–52459, 2018. [Online]. Available: https://ieeexplore.ieee.org/document/8467327/

[34] R. De Gaudenzi, "An integrated LEO communication and PNT system for beyond 5G NTN," *Int. J. Satellite Commun. Netw.*, Feb. 2025.

[35] S. M. Kay, *Fundamentals of Statistical Signal Processing* (Prentice Hall Signal Processing Series). Englewood Cliffs, NJ, USA: Prentice-Hall, 1993.

[36] T. He and Z. Ma, "Proposed OFDM modulation for future generations of GNSS signal system," *J. Navig.*, vol. 69, no. 5, pp. 971–990, Sep. 2016. [Online]. Available: https://www.cambridge.org/core/journals/journal-of-navigation/article/proposed-ofdm-modulation-for-future-generations-of-gnss-signal-system/1389D99AB66AC3D4C64E0031BA46A685#

[37] J. Su, J. Su, Q. Yi, C. Wu, and W. Hou, "Design and performance evaluation of a novel ranging signal based on an LEO satellite communication constellation," *Geo-Spat. Inf. Sci.*, vol. 26, pp. 107–124, Jan. 2023. [Online]. Available: https://www.tandfonline.com/doi/abs/10.1080/10095020.2022.2121229

[38] K. Han, J. Yin, Z. Deng, J. Dong, S. Tang, and Z. Ma, "The base stationsŠ networking scheme and spreading code optimization strategy of TC-OFDM," in *Proc. China Satellite Navig. Conf. (CSNC)*, 2020, pp. 485–496. [Online]. Available: https://link.springer.com/chapter/10.1007/978-981-15-3707-3_46

[39] D. Egea-Roca, J. López-Salcedo, G. Seco-Granados, and E. Falletti, "Performance analysis of a multi-slope chirp spread spectrum signal for PNT in a LEO constellation," in *Proc. 10th Workshop Satellite Navig. Technol. (NAVITEC)*, 2022, pp. 1–9. [Online]. Available: https://ieeexplore.ieee.org/document/9847559

[40] F. Fabra, D. EgeaŰRoca, J. A. LópezŰSalcedo, and G. SecoŰGranados, "Analysis on signals for LEO-PNT beyond GNSS," in *Proc. 32nd Eur. Signal Process. Conf. (EUSIPCO)*, 2024, pp. 1237–1241. [Online]. Available: https://ieeexplore.ieee.org/document/10714965/

[41] E. Yuan, W. Qi, P. Liu, L. Wei, and L. Chen, "Ranging method for navigation based on high-speed frequency-hopping signal," *IEEE Access*, vol. 6, pp. 4308–4320, 2018. [Online]. Available: https://ieeexplore.ieee.org/document/8241378

[42] D. Fu, H. Lin, Y. Meng, J. Peng, G. Ou, and S. Wang, "Delay–doppler block division multiplexing: An integrated navigation and communication waveform for LEO PNT," *Remote Sens.*, vol. 17, no. 7, p. 1270, Apr. 2025. [Online]. Available: https://www.mdpi.com/2072-4292/17/7/1270

[43] H. Chen et al., "Modeling and analysis of OFDM-based 5G/6G localization under hardware impairments," *IEEE Trans. Wireless Commun.*, vol. 23, no. 7, pp. 7319–7333, Jul. 2024. [Online]. Available: https://ieeexplore.ieee.org/document/10355872

[44] A. Gonzalez-Garrido, J. Querol, and S. Chatzinotas, "5G positioning reference signal configuration for integrated terrestrial/non-terrestrial network scenario," in *Proc. IEEE/ION Posit., Locat. Navig. Symp. (PLANS)*, 2023, pp. 1136–1142. [Online]. Available: https://ieeexplore.ieee.org/document/10140024/

[45] J. J. Van De Beek, M. Sandell, and P. Borjesson, "ML estimation of time and frequency offset in OFDM systems," *IEEE Trans. Signal Process.*, vol. 45, no. 7, pp. 1800–1805, Jul. 1997. [Online]. Available: http://ieeexplore.ieee.org/document/599949/

[46] *NR; Physical Channels and Modulation*, 3GPP Standard TS 38.211, 2024. [Online]. Available: https://portal.3gpp.org/desktopmodules/Specifications/SpecificationDetails.aspx?specificationId=3213

[47] E. Juan, M. Lauridsen, J. Wigard, and P. Mogensen, "Handover solutions for 5G low-earth orbit satellite networks," *IEEE Access*, vol. 10, pp. 93309–93325, 2022.

[48] E. Kaplan and C. Hegarty, *Understanding GPS: Principles and Applications* (Artech House Mobile Communications). Norwood, MA, USA: Artech House, 2006.

[49] K. Schuler and W. Wiesbeck, "Tapering of multitransmit digital beamforming arrays," *IEEE Trans. Antennas Propag.*, vol. 56, no. 7, pp. 2125–2127, Jul. 2008. [Online]. Available: https://ieeexplore.ieee.org/abstract/document/4558316

[50] A. B. Ayed, P. Mitran, and S. Boumaiza, "Novel algorithm to synthesize the tapering profile for enhanced linearization of RF beamforming arrays over a wide steering range," *IEEE Trans. Microw. Theory Tech.*, vol. 71, no. 8, pp. 3691–3700, Aug. 2023. [Online]. Available: https://ieeexplore.ieee.org/abstract/document/10066144

[51] H. Cox and H. Lai, "Sub-aperture beam-based adaptive beamforming for large dynamic arrays," in *Proc. Conf. Record 38th Asilomar Conf. Signals, Syst. Comput.*, 2004, pp. 2355–2358. [Online]. Available: https://ieeexplore.ieee.org/abstract/document/1399590

[52] K. Plimon, J. Ebert, H. Schlemmer, A. Mengali, and A. Ginesi, "Subset precoding and tapering on phased arrays for high throughput satellite systems," in *Proc. 13th Int. Symp. Commun. Syst., Netw. Digit. Signal Process. (CSNDSP)*, 2022, pp. 115–120. [Online]. Available: https://ieeexplore.ieee.org/abstract/document/9907918

[53] D. Parker and D. C. Zimmermann, "Phased arrays—Part 1: Theory and architectures," *IEEE Trans. Microw. Theory Tech.*, vol. 50, no. 3, pp. 678–687, Mar. 2002. [Online]. Available: https://ieeexplore.ieee.org/abstract/document/989953

[54] W. Hong et al., "Multibeam antenna technologies for 5G wireless communications," *IEEE Trans. Antennas Propag.*, vol. 65, no. 12, pp. 6231–6249, Dec. 2017. [Online]. Available: https://ieeexplore.ieee.org/abstract/document/7942144

[55] T. Schmidl and D. C. Cox, "Robust frequency and timing synchronization for OFDM," *IEEE Trans. Commun.*, vol. 45, no. 12, pp. 1613–1621, Dec. 1997. [Online]. Available: http://ieeexplore.ieee.org/document/650240/

[56] Y. Sun, Y. Zhai, W. Wu, P. Si, and F. R. Yu, "Handover for multi-beam LEO satellite networks: A multi-objective reinforcement learning method," *IEEE Commun. Lett.*, vol. 28, no. 12, pp. 2834–2838, Dec. 2024. [Online]. Available: https://ieeexplore.ieee.org/abstract/document/10700698

[57] "Solutions for NR to support non-terrestrial networks (NTN)," 3GPP, Sophia Antipolis, France, Rep. 38.821, Jun. 2021.

[58] J. M. Gongora-Torres, C. Vargas-Rosales, A. Aragón-Zavala, and R. Villalpando-Hernandez, "Link budget analysis for LEO satellites based on the statistics of the elevation angle," *IEEE Access*, vol. 10, pp. 14518–14528, 2022. [Online]. Available: https://ieeexplore.ieee.org/abstract/document/9698051

[59] B. Zheng, Y.-C. Yu, J.-Y. Wang, and C. Ding, "Inter-beam handover schemes for LEO satellites in 5G satellite–terrestrial integrated networks," *Phys. Commun.*, vol. 67, Dec. 2024, Art. no. 102525. [Online]. Available: https://www.sciencedirect.com/science/article/pii/S187449072400243X

[60] O. B. Yahia et al., "Evolution of high throughput satellite systems: Vision, requirements, and key technologies," 2023, *arXiv:2310.04389*.

[61] F. Vidal, H. Legay, G. Goussetis, S. Tubau, and J.-D. Gayrard, "Flexibility/complexity trade-offs in payload design," in *Non-Geostationary Satellite Communications Systems*. London, U.K.: Inst. Eng. Technol., 2024, pp. 113–142. [Online]. Available: https://digital-library.theiet.org/doi/10.1049/PBTE105E_ch6

[62] P. K. Bailleul, "A new era in elemental digital beamforming for spaceborne communications phased arrays," *Proc. IEEE*, vol. 104, no. 3, pp. 623–632, Mar. 2016. [Online]. Available: https://ieeexplore.ieee.org/abstract/document/7389972

[63] "Technical specification group radio access network; solutions for NR to support non-terrestrial networks (NTN); (Release 15), Version 15.2.0," 3GPP, Sophia Antipolis, France, Rep. TR 38.821, 2018.

[64] R. D. Gaudenzi and M. Luise, "Revisiting band-limited DS/SS signal design for GNSS," in *Proc. 11th Workshop Satellite Navig. Technol. (NAVITEC)*, 2024, pp. 1–5. [Online]. Available: https://ieeexplore.ieee.org/abstract/document/10843514

[65] F. Rinaldi et al., "Broadcasting services over 5G NR enabled multi-beam non-terrestrial networks," *IEEE Trans. Broadcast.*, vol. 67, no. 1, pp. 33–45, Mar. 2021. [Online]. Available: https://ieeexplore.ieee.org/document/9107401

[66] M. Ibarra, A. G. Andrade, M. A. Panduro, and A. L. Mendez, "Design of antenna arrays for isoflux radiation in satellite systems," in *Proc. IEEE 33rd Int. Perform. Comput. Commun. Conf. (IPCCC)*, 2014, pp. 1–2. [Online]. Available: https://ieeexplore.ieee.org/abstract/document/7017028

[67] L. Italiano, B. C. Tedeschini, M. Brambilla, H. Huang, M. Nicoli, and H. Wymeersch, "A tutorial on 5G positioning," *IEEE IEEE Commun. Surveys Tuts.*, early access, Aug. 23, 2024, doi: 10.1109/COMST.2024.3449031.

[68] M. Yuan, X. Tang, and G. Ou, "Authenticating GNSS civilian signals: A survey," *Satellite Navig.*, vol. 4, no. 1, p. 6, Dec. 2023. [Online]. Available: https://doi.org/10.1186/s43020-023-00094-6

[69] S. Varrette, H. Cartiaux, S. Peter, E. Kieffer, T. Valette, and A. Olloh, "Management of an academic HPC & research computing facility: The ULHPC experience 2.0," in *Proc. 6th ACM High Perform. Comput. Clust. Technol. Conf. (HPCCT)*, 2022, pp. 14–24.

ALEJANDRO GONZALEZ-GARRIDO (Student Member, IEEE) received the integrated degree and the M.Sc. degree in telecommunication engineering in 2015. He is currently pursuing the Ph.D. degree with the SIGCOM Group of SnT, University of Luxembourg, specializing in hybrid GNSS and 5G PNT systems using non-terrestrial networks. He have professional experience in the timing and synchronization industry, satellite design, and network operations.

JORGE QUEROL (Member, IEEE) received the Ph.D. degree in telecommunication engineering from the Polytechnic University of Catalonia (UPC-BarcelonaTech), Barcelona, Spain, in 2018. He joined the Signal Processing and Satellite Communications Group, headed by Prof. B. Ottersten, and he will be working with Dr. S. Chatzinotas. His research interests include Software-Defined Radios, real-time signal processing, satellite communications, satellite navigation, and remote sensing.

HENK WYMEERSCH (Fellow, IEEE) received the Ph.D. degree in electrical engineering/applied sciences from Ghent University, Belgium, in 2005. He is currently a Professor of Communication Systems with the Department of Electrical Engineering, Chalmers University of Technology, Sweden. His current research interests include the convergence of communication and sensing, in a 5G and beyond 5G context. He is a Senior Member of the IEEE Signal Processing Magazine Editorial Board. From 2019 to 2021, he was an IEEE Distinguished Lecturer with the Vehicular Technology Society.

SYMEON CHATZINOTAS (Fellow, IEEE) received the M.Eng. degree in telecommunications from the Aristotle University of Thessaloniki, Greece, in 2003, and the M.Sc. and Ph.D. degrees in electronic engineering from the University of Surrey, U.K., in 2006 and 2009, respectively.

He is currently a Full Professor, the Chief Scientist I, and the Head of the Research Group SIGCOM, Interdisciplinary Centre for Security, Reliability and Trust, University of Luxembourg. In the past, he has lectured as a Visiting Professor with the University of Parma, Italy, and contributed in numerous research and development projects for the Institute of Informatics and Telecommunications, National Center for Scientific Research ''Demokritos," the Institute of Telematics and Informatics, the Center of Research and Technology Hellas and Mobile Communications Research Group, the Center of Communication Systems Research, University of Surrey. He has authored more than 700 technical papers in refereed international journals, conferences, and scientific books. He has received numerous awards and recognitions, including the IEEE Fellowship and an IEEE Distinguished Contributions Award. He is currently in the editorial board of the IEEE TRANSACTIONS ON COMMUNICATIONS, IEEE OPEN JOURNAL OF VEHICULAR TECHNOLOGY, and the *International Journal of Satellite Communications and Networking*.